Phenomenology of Spatio-Temporal Chaos

James P. Crutchfield
Physics Department
University of California
Berkeley, California 94720
USA

and

Kunihiko Kaneko
Institute of Physics
College of Arts and Sciences
University of Tokyo
Tokyo 153, JAPAN

1. COMPLEXITY AND STATISTICAL MECHANICS OF DETERMINISTIC BEHAVIOR

The continuing advancement of science and technology depends to a large degree on the development of a theoretical framework for and a practical appreciation of highly complex systems, as they occur in natural and human-engineered systems. One important avenue of study in this larger endeavor is the investigation of nonlinear dynamical systems with spatially-distributed degrees of freedom. The latter is not an entirely new line of inquiry, rather it has flourished on a number of research frontiers over the last several decades. Nonetheless, the recent rapid progress in understanding unpredictable, or *chaotic,* systems in low dimensions suggests a new look at spatial nonlinear dynamics. This is the goal of the present discussion. Here we review some of the rich phenomenology found in spatial systems composed of a large number of low-dimensional chaotic systems.* The diversity of behavior in this simple class of *lattice dynamical systems* is often reminiscent of well-known behavior in a range of fields in which spatial dynamics plays a significant role.

To motivate our inquiry into spatial dynamical systems, it is worthwhile to recall some fields where spatial extent is an important aspect of behavior. We comment briefly on fluid turbulence, ergodicity in statistical mechanics, pattern formation in natural systems, solitons, excitations in solids, neural networks, parallel computation, and, lastly, digital signal processing.

The long-standing problem of fluid turbulence, especially as it relates to flows labeled ''fully-developed'', has been a recurrent motivation in the development of nonlinear dynamics. Chaos, as it is now understood, provides a suggestive conceptual framework: the state space representation of a turbulent flow may be a strange attractor.[3,4] Upon closer inspection, however, one realizes that chaos indicates nothing about spatial structure. This is a significant omission, as corroborated by a number of allied questions at the forefront of turbulence experiments: the mechanism by which fluctuations may be spatially amplified; the occurrence of spatial patterns amidst turbulence; intermittency in space and time;[5] and dislocation dynamics.[6] On the

*This chapter reviews the authors' work on spatial chaos during the last four years.[1,2] Much of JPC's work presented here, although already presented in lectures, is previously unpublished. Reference's to

theoretical front, tools from dynamical systems theory lead to estimates of the dimensionality of fully-developed turbulence and the existence of the Lyapunov spectra density has been investigated for the Navier-Stokes equation.[7] Unfortunately, at present there is little geometric understanding of how the latter abstract results bear on the former experimental observations of complex spatial dynamics.

In the classical picture of statistical mechanics, it is believed that a large number of degrees of freedom is necessary for ergodicity. The recent paradigm of low-dimensional chaos has shown that a limited statistical mechanics can be constructed for systems with few degrees of freedom, if sufficient nonlinearity exists. In these low-dimensional systems, however, the distribution of states is far from "equipartition" and is replete with highly-probable states, even "singularities". The exact requirements of equipartition are not met, except for a small set of atypical chaotic systems. Furthermore, it is not clear how these distributions behave as the number of degrees of freedom grows in the thermodynamic limit nor is it self-evident how spatial extent affects their spatial structure. Perhaps both elements are necessary for the proper foundation of statistical mechanics: the creation of local chaos by a low-dimensional mechanism and the spatial transmission of information and energy to a large number of modes.

Numerical investigations[8] of ergodicity in a nonlinear chain of oscillators led to the discovery of particle-like *solitons*.[9] That continuum systems admit stable, localized excitations has provided a powerful metaphor in a number of disciplines, such as, elementary particles, excitations in solids, and water waves, to name a few. In a rigorous sense, the term "soliton" refers only to energy conserving dynamics that admits dispersionless collisions of propagating perturbations. In a rough sense, though, the term can be usefully applied to any stable elementary excitation. With this in mind, it is helpful to study the interactions among "solitons" in a wide range of dissipative systems in order to understand the common features of their structure and persistent stability. In some systems, solitons are seen to pair-create and annihilate in a chaotic or turbulent fashion. It is just such highly nonlinear phenomena that are inaccessible, at present anyway, to entirely analytical methods.

Many phenomena in solid state physics occur in spatially-extended systems and are associated with the interaction and propagation of elementary excitations. Typically, these systems are nonlinear so that one may not analytically investigate the full range of observed behavior. Examples abound: spin wave turbulence in ferrites,[10,11] the appearance of complex domains and walls in two-dimensional magnets,[12] magnetic bubble lattices,[13] strip and arrays of Josephson junctions, charge density waves,[14] nonlinear transmission lines,[15] coupled systems of optically bistable elements, video feedback, chains of electronic nonlinear oscillators,[16,17] electron-hole plasmas,[18] and ferrofluid dynamics.[19,20]

The formation of spatial patterns plays an important role in natural systems.[21] Heuristically, one pervasive mechanism responsible for this involves a spatially-local instability and its propagation by diffusion or transport. This has been studied in spinodal decomposition, in dendritic growth,[22] in video feedback,[23] and in more general reaction-

---

KK's publications can be found throughout the text.

diffusion systems. The latter are used to model chemical[24] and biological[25] oscillations and morphogenesis.[26] Turbulent, spatially-complex growth is a common phenomenon in these fields.

The recent extension of associative memory models[27] to "neural networks" relies on the basin structure of fixed point attractors to store and retrieve patterns.[28,29] This has provided a model for biological computation that employs some of the geometric flavor of dynamical systems theory. Indeed, these networks are lattice dynamical systems with a high "interconnectivity" dimension (Defined below). At the present, most studies focus on highly-discretized cellular-automata-like architecture with binary-thresholding local dynamics. To date, these models allow a single neuron only two, or a few, states and it cannot have its own complex time-dependent dynamics. This is in direct contrast to recent experiments that indicate single neurons can have rich dynamics: more than a few states can be stored and even chaotic behavior may appear. The other extreme has been to investigate neural networks as pattern generating systems, ignoring their computational capabilities.[30] The study of a network of local nonlinear systems as presented here will be an important prerequisite to modeling and interpretation of realistic neural networks.

The coincidence of technological advances and the need for substantial improvements in computational speed and storage has lead to the construction of very large and highly parallel computers. One of the interesting problems presented by these distributed processing systems is how to program them efficiently. While at one time an important motivating factor in their development, simulations of spatially-extended dynamics may also lead to algorithmic metaphors for understanding more complex processing in highly parallel machines. For example, lattice dynamical systems provide a quantitative test-bed for studying the informational architecture of parallel machines and for the further development of parallel computation theory.

Finally, we note that many digital signal processing algorithms admit a quasi-spatial lattice formulation,[31] even if the signal does not explicitly depend on space. The most often-used processing methods are linear: frequency domain filtering, adaptive linear models, power spectral density estimates, and so on. Digital signal processing is commonly described using signal "flow" graphs. It is not mere coincidence that a similar descriptive statistical technique for chaos and especially spatially-extended dynamical systems is based on the "flow" of information.[32] Although these two perspectives are not so different in intent, in digital signal processing the prototype problems fall short of addressing genuine nonlinearity. In contrast, in nonlinear dynamics the attempt is to describe manifestly nonlinear behavior and its qualitative dynamics in terms of the flow of information. In digital signal processing the computational elements are clear; unfortunately, dynamical systems theory provides little insight at present into the underlying state space structures.

Nonetheless, some insight is obtained in viewing the action of nonlinear spatial dynamics on input patterns, or initial conditions, as analogous digital signal processing operations. Conversely, the study of nonlinear lattice dynamics should bring a concomitant broadening of our understanding and use of digital signal processing to encompass nonlinear problems. Digital and analog phase locked loops are concrete examples of a fruitful cross fertilization. To end this digression, we mention two

questions that shall be of increasing importance to designing with dynamical systems. In what sense can a, lattice or any other, dynamical system be said to be performing a ''computation''? And, what are the associated state space structures for this? The following discussion of a wide range of spatio-temporal dynamics should be seen as an indirect, preliminary attempt to ''engineer'' complex nonlinear dynamics, by first appreciating the diversity of tools.

Dynamical systems theory developed during the last decade largely through the study of low-dimensional systems. In the pursuit of an equivalent geometric understanding in the fields just described, however, the progress to date forms just the first steps. Previous investigations of (say) low-dimensional chaos, although suggestive, by no means provide a useful, let alone complete, picture at present. To be of use to these fields, dynamical systems theory must be extended to space *and* time. This chapter attempts to do this along a particular line of inquiry.

In the following, we present a class of prototypes for space-time dynamics and explore the qualitative behavior of some of its members. Given the present state of our ignorance, we must start with a heuristic and phenomenological investigative style based on extensive simulations and using several different methods of visualizing the high-dimensional dynamics.* The logical and complementary next step beyond this is the development of thermodynamic quantifiers appropriate to spatio-temporal statistical behavior. These include extensive and intensive forms of dimension, entropy, and mutual information. To complete the geometric picture of the deterministic dynamics involved, these quantifiers must then be related back to the pattern dynamics. Lastly, to provide the link from theory and numerical work to experiments, ''reconstruction'' methods[33] must be generalized to space and time. The following sections present only a brief review of the phenomenological aspects of spatio-temporal chaos. The other steps just outlined can be found in other work by the present authors.[32,34,35,36]

The basic definitions of lattice dynamical systems are laid out, initially, along with the characteristics that distinguish them from arbitrary systems. The phenomenology starts with period-doubling lattices, behavior that is relatively easy to anticipate from knowing the structure of the local dynamics. Next, the competition between spatial modes illustrates a new route to spatio-temporal chaos via quasi-periodicity, that is not so apparent. A wide range of particle dynamics is then investigated in soliton-bearing lattices. Several types of intermittency are then covered; most noteworthy is a new type due to the competition of spatial patterns. Spatial amplification of fluctuations is studied in unidirectionally-coupled systems. Finally, the occurrence of apparently chaotic, but very-long-lived transient patterns is illustrated in a lattice model of a dripping handrail.

---

*The simulations were performed with *lds*, a lattice dynamical system simulator. Currently, *lds* runs on Sun Microsystem Workstations. Given sufficient interest, this simulator will be made available for Apple Macintosh II workstations. Contact the first author for further information on the simulator. Arpanet/Internet mail address: chaos@gojira.berkeley.edu.

2. LATTICE DYNAMICAL SYSTEMS: PROTOTYPES FOR SPATIO-TEMPORAL COMPLEXITY

The difficulty with a naive dynamical systems interpretation of spatially-extended systems lies not so much in the raw number of degrees of freedom, which is problematic, but that the degrees of freedom are spatially distributed and that any useful description must incorporate this structure. Indeed, the spatial nature of these systems is a translation symmetry. This symmetry in turn suggests the possibility of a description of complex spatially-extended systems simpler than that of systems with the same number of degrees of freedom which are not spatially-extended. In this section, we shall first discuss the nature of a spatial system and distinguish this from a general dynamical system. Then, we define the class of lattice dynamical systems to be studied and the possible boundary and initial conditions.

2.1. Restriction to Spatial Lattices

In general N-dimensional dynamical systems, the connection among N variables can take any form depending on the problem. With lattice dynamical systems, we treat mainly systems with ''spatial translation'' invariance, which gives a restriction to the coupling among variables and indicates that the individual variables are somehow comparable. We can, for example, compute ''field'' averages over the local variables.

This distinction can be clarified by comparing a spatially-extended system to an arbitrary dynamical system with the same (large) number degrees of freedom. (See figure 1.) From this one sees that spatially-extended systems are a subset of all possible dynamical systems restricted by the symmetry of ''local'' coupling of degrees of freedom. This symmetry is an isotropic spatial invariance. In contrast, an arbitrary system may have couplings between any two degrees of freedom, independent of any symmetry. It can be more complex in behavior than a comparable spatially-extended system in that information can be transmitted more rapidly to a large number of degrees of freedom in the same time.

A coarse measure for this comparison may be developed for countably-infinite dynamical systems as follows. We shall not discuss the case of continuum systems, such as partial differential equations. We define the *interconnectivity dimension* D_{inter} of a dynamical system with arbitrarily many degrees of freedom as the asymptotic growth rate of the number of degrees of freedom within a given *interconnectivity distance* r. The interconnectivity distance $r(p,q)$ between two degrees of freedom p and q is the number of links along the shortest path between nodes p and q in the connected graph describing the coupling between the degrees of freedom. The adjacency matrix of this graph is obtained from the dynamical system's Jacobian. Considering a single reference degree of freedom p, for an infinite system, we have

$$D_{inter}(p) = \lim_{r \to \infty} \frac{\log nhbr(r)}{log(r)} ,$$

where nhbr(r) is the total number of neighbors within a ''radius'' r of p. The interconnectivity dimension is averaged over the entire system starting at each degree of

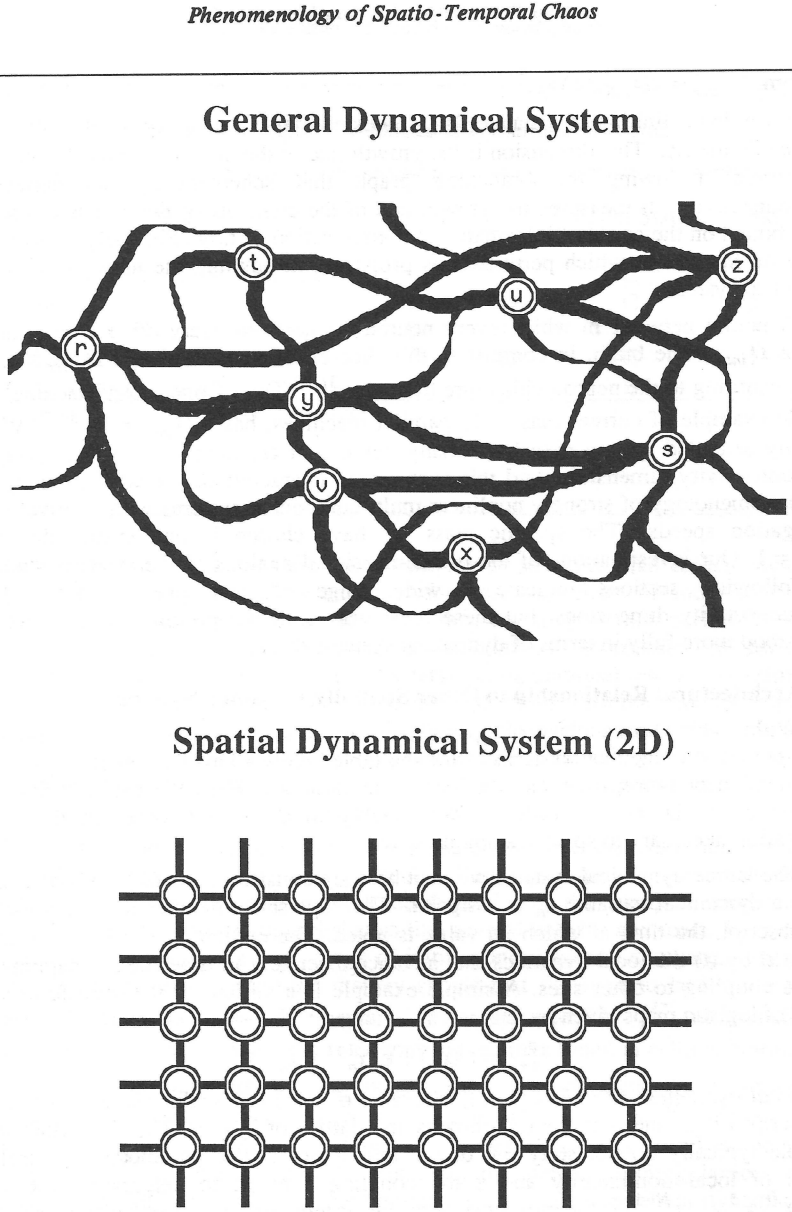

Figure 1. Arbitrary versus spatial dynamical systems. A schematic representation where the circular nodes denote the system variables and the heavy lines, connection pathways between them.

freedom: $D_{inter} = \langle D_{inter}(p) \rangle_p$.*

With this definition of distance, D_{inter} does not depend on a notion of spatial extent or a spatial metric. This dimension is the growth rate of the number of possible paths one may travel following the branching graph that schematically summarizes the interconnectivity. It measures the growth rate of the elements of this graph and so is an upper bound on the speed of information communication or flow. Similarly, it is an upper bound on the rate at which perturbations propagate throughout the network of coupled dynamical systems.

A neural network in which every neuron connects to every other would have an infinite D_{inter}. The brain, in contrast to this theoretical extreme, has a $D_{inter} \simeq$ 100 to 1000 according to the neuroarchitecture literature.[37,38] The "Connection Machine", as a notable example of current massively parallel machines, has a $D_{inter} = 14$.[39,40] While a spatially-extended system may have many degrees of freedom, it also has a very low interconnectivity dimension. And this is the main characteristic we wish to study here: the phenomenology of strongly nonlinear multi-component systems with relatively small propagation speeds. The specific class we have chosen is one spatial dimension, $D_{inter} = 1$. Our investigations of the two-dimensional analogs of the systems studied in the following sections indicate a wide range of new phenomena in higher interconnectivity dimensions, but these must wait until the present models have been understood more fully in terms of dynamical systems theory.

2.2. Architectural Relationship to Other Spatially-Extended Systems

Within the chosen class of spatially-extended systems, there is a hierarchy of spatio-temporal dynamical systems. (See the table below.) This derives from choices of discretization of space, time, and the local state variables. The table lists just five of the possible 8 subclasses and orders them roughly in decreasing order in the amount information necessary to specify a unique state.

The lattice dynamical systems we treat here are constructed as follows. On a spatial lattice a dynamical variable x_n^i is assigned. The superscript denotes the site's location; the subscript, the time at which its value is noted. The evolution of a local variable is governed by (i) the local dynamics that advance discretely in time (i.e., a mapping) and (ii) the coupling to other sites. A simple example is a variant of the *logistic lattice:* a lattice of logistic maps given by

$$x_{n+1}^i = f(x_n^i) + \varepsilon (x_n^{i+1} + x_n^{i-1})$$

with *local dynamics:* $f(x) = rx(1-x)$, **where** $x \in [0,1]$ is a scalar and $r \in [0,4]$. The superscript i is an index in the one-dimensional lattice of N sites. The site values in this example typically do not stray out of the unit interval. The parameter r controls the degree of local nonlinearity and ε the coupling strength to neighbors. The vector $\vec{x}_n = (x_n^0, x_n^1, \ldots, x_n^{N-1})$ is the current state of the system; also called its *pattern* or *field.*

*We have given here the "topological" version of D_{inter}. There is, naturally, a "metric" version, in the sense used for entropies, and, indeed, an entire Renyi spectrum, of similar dimensions. In these, the interconnecting links are given weights. These weights might describe distance on some manifold or, perhaps, connection strengths as in neural networks.

Hierarchy of Spatially-Extended Dynamical Systems				
Model	Space	Time	Local State	Class
Partial Differential Equations	C	C	C	7
Iterated Functional Equations	C	D	C	5
Oscillator Chains	D	C	C	3
Lattice Dynamical Systems	D	D	C	1
Cellular Automata	D	D	D	0

D = Discrete
C = Continuous

Lattice dynamical systems are more complex in structure than cellular automata, having continuous state variables and therefore the capability of local information production. Being discrete in time and space, they are simpler than partial differential equations which require a multiply-infinite amount of information (a continuous function) to specify a state (and substantially larger computational resources to simulate). While the relationship between the dynamics of these different model classes is traditionally the concern of numerical analysts, there are undoubtedly important mathematical and physical insights to be gained from understanding the hierarchy itself. At the very least, this would allow one to intelligently choose the appropriate mathematical models for a given physical problem.

Without a complete delineation of the hierarchy, one can still indicate certain similarities in behavior and show particular limiting cases for which there is a connection. The binary space-time symbolic dynamics of the one-dimensional logistic lattice, to take a concrete example, behaves like several cellular automata. For example, in the period 2 regime, for a wide range of initial conditions and comparing asymptotic behavior, a binary-state space-time display shows that the logistic lattice obeys one-dimensional nearest-neighbor "elementary" automata rule 23.*[41,42] Additionally, the lattice system exhibits domain walls analogous to the kinks found in cellular automata.[43]

A more interesting connection, though, can be made with chains of coupled oscillators. Many oscillators undergo a period-doubling cascade.[44,45,46] A weakly coupled chain of these oscillators exhibits the universal features found in the period-doubling lattices described below. In this case, the period-doubling lattices can be considered as a Poincaré section of the continuous-time oscillator chain dynamics. This qualitative correspondence has been numerically verified for a modest length chain of Rössler oscillators[47] by one of the authors.

*Elementary cellular automata rule 23 evolves from initial patterns so that (i) the behavior is overall temporal period 2, (ii) isolated 0's and 1's disappear, and (iii) domain walls are maintained.

In the context of continuum physical problems, the use of partial differential equations is standard. Recently, much numerical work has begun on chaotic spatio-temporal behavior in nonlinear partial differential equations.[48,49] A few connections with this work should be mentioned. A forward-difference discretization of the real time-dependent Ginzburg-Landau equation yields a period-doubling lattice. As does the same for Fisher's equation. Huerre and Moon[50] have studied numerically the continuum limit of the complex time-dependent Ginzburg-Landau equation. They found a quasi-periodic route to chaos via the thickening of tori. With the simple addition of another control parameter, the logistic lattice itself can be thought of as an iterative solution of the real time-independent Ginzburg-Landau equation. Bishop and collaborators[51] have performed extensive numerical simulations of the driven, damped Sine-Gordon partial differential equation. This system is often modeled by a chain of coupled pendula and in an appropriate regime, the period-doubling lattices describe a chain of driven damped pendula, each of which exhibits period-doubling. A more faithful lattice analogue of the Sine-Gordon PDE is found by replacing the logistic map with local phase dynamics using circle maps. As shown later, the coupled circle lattice shows kink-antikink propagation and chaotic pair collisions that look quite similar to behavior found in the Sine-Gordon PDE with damping and external forcing.

Finally, the architectural connection mentioned already with reaction-diffusion PDEs is quite close as the latter are essentially the superposition of local nonlinear dynamics (reaction) and the spatial coupling (diffusion). In some limits a direct connection can be established.[52] Other behavioral similarities with members of the spatial hierarchy will become quite apparent in the following sections on lattice phenomenology.

2.3. Choice of Local Dynamics

One may select from a variety of discrete time systems for the local dynamics. Since some classes of low-dimensional maps have been investigated extensively, we select them as the local dynamics of our lattice systems. Typical examples include

(i) the logistic map $f(x) = rx(1-x)$, as mentioned above;

(ii) the circle map $f(x) = \omega + x + k\ sin(2\pi x)$; and

(iii) piecewise linear functions, such as the shift or tent maps.

For two local variables, one might use 2-dimensional maps, such as Hénon's or Lozi's dissipative maps or the standard map. The latter, with proper coupling, forms a symplectic lattice. In the present paper, we restrict ourselves to local dynamics of a single variable.

2.4. Coupling Classes

Similarly, there is wide latitude in choosing the coupling form. It can be local, in which the dynamics of a site is determined by the variables at neighboring sites; or nonlocal, in which a site is determined by a set of sites possibly far from the site. The coupling radius must also be selected: the extreme case of short range is nearest-neighbor coupling. We shall restrict ourselves only to the nearest neighbor coupling. Thus, the dynamics of site i is affected only by the variables at site i-1, i, and i+1.

With these restrictions and a few additional ones, we end up with the following lattice dynamical system that will be the subject of investigation in this paper:

$$x_{n+1}^i = f(x_n^i) + \varepsilon_0 g(x_n^i) + \varepsilon_R g(x_n^{i+1}) + \varepsilon_L g(x_n^{i-1})$$

The vector $\vec{\varepsilon} = (\varepsilon_0, \varepsilon_L, \varepsilon_R)$ is the *coupling kernel*. The next step is the choice of the function g(x), the *coupling dynamics*. We have studied the cases of "linear-coupling" g(x) = x, "future-coupled" g(x) = f(x),[53] and many other special choices, such as nonlinear couplings and larger range kernels as for "lateral inhibition".

The future-coupling form is particularly useful for several reasons. First, each site value remains in the same range as for the isolated map. The lattices are conveniently "normalized" by this property. Second, the "pre-iteration" of the neighboring sites before they are added to the central site provides a closer approximation to a stroboscopic view of an analogous continuous-time oscillator chain; the iteration being a better approximation of the neighbors current state than simply using their values from the previous cycle. This feature also leads to the suppression of the anti-correlated spatial configurations mentioned below. Here we mostly report on the linear and future coupling cases, as these are rather simple and include a representative range of behavior from these other possible couplings.

The last choice is the symmetry of the coupling kernel. This is determined by the coupling values ε_0, ε_R, and ε_L. In the following, we present three cases

(i) Additive coupling: $\varepsilon_0 = 0$, $\varepsilon_R = \varepsilon_L$;

(ii) Laplacian coupling: $-\frac{\varepsilon_0}{2} = \varepsilon_R = \varepsilon_L$;

(iii) Totalistic coupling: $\varepsilon_0 = -\frac{2}{3}$, $\varepsilon_R = \varepsilon_L = \frac{1}{3}$; and

(iv) Uni-directional coupling: $-\varepsilon_0 = \varepsilon_L$ and $\varepsilon_R = 0$.

The first three types are models for the system with symmetric diffusion, while the latter corresponds to asymmetric coupling[1] as found in modeling of the open flows.[54]

2.5. Boundary Conditions

We can choose a number of different boundary conditions depending on the problem: fixed, periodic, free, noise or periodically driven, and so on. We restrict ourselves largely to periodic boundary conditions, unless otherwise explicitly noted. The qualitative dynamics, however, typically is independent of boundary conditions, for sufficiently large lattices.

2.6. Initial Conditions

For initial conditions, spatially periodic functions, e.g., $\sin(2\pi kiN^{-1})$, or uniformly distributed random functions with given mean and standard deviation are employed. The latter choice is convenient to select out a statistically probable pattern and so to study "generic" behavior. One problem with this type, though, is that it does not admit a natural continuum limit, unless spatially band-limited.

With prototype models and their boundary and initial conditions specified, we turn now to particular lattices and their behavior. From extensive simulations we have

selected a range of phenomena that is indicative of the wealth of complex dynamics in the wider class of lattice dynamical systems. The first example derives from period-doubling local dynamics and serves as a simple entré into spatio-temporal dynamics, the local dynamics being familiar and widely studied. The behavior of succeeding examples, such as anti-ferromagnetic transitions, phase lattices, pattern competition intermittency, and transient spatial chaos, tend to be less easily deduced from the dynamics of their constituents.

3. PERIOD-DOUBLING LATTICES

In the following section, we will study the coupled logistic lattice: specifically, the period-doubling of spatially "coherent" *domains* and the *kinks* that separate them. The model is given by the local dynamics $f(x) = rx(1-x)$ and the lattice equation is constructed with future Laplacian coupling

$$x_{n+1}^i = (1-\varepsilon)f(x_n^i) + \frac{\varepsilon}{2}\{f(x_n^{i+1}) + f(x_n^{i-1})\},$$

with linear Laplacian coupling

$$x_{n+1}^i = f(x_n^i) + \frac{\varepsilon}{2}(x_n^{i+1} + x_n^{i-1} - 2x_n^i),$$

or with simple additive coupling

$$x_{n+1}^i = f(x_n^i) + \varepsilon(x_n^{i+1} + x_n^{i-1}).$$

As the nonlinearity r is increased, the single logistic map shows the classic period-doubling cascade to chaos. In the lattice equation, this local temporal period-doubling induces spatial domain structures of phase coherent sites. *Domains* are taken to be regions in space in which the site values are correlated to some specified degree in space and time. Depending on the context, this correlation can take the form of an explicit translation symmetry (all site values are equal) or perhaps a combination period-2 space and time translation symmetry. These regions are separated by *walls,* or *kinks,* that develop at sites whose initial amplitudes are near unstable fixed x^* points of the local dynamics: $f^P(x^*) = x^*$, for some period $P = 2^k$, for example. As the local dynamics period-doubles with r or ε, the spatial wavelengths also decrease in a regular manner. Amplitude plots are shown in figures 2 through 5, where we see the kink and anti-kink structures caused by the temporal period-doubling: period 4 in figure 2 (top) and period-8 for figure 2 (bottom).[1,53,55]

Examples of chaotic states are shown in figures 3 and 4, where the patterns through 16 time steps are shown after the transients have died out. We note that some low-periodicity domain structure remains even if the patterns are chaotic. If the nonlinearity is small, the domain boundaries cannot move. In this case, the domain size distribution depends on the initial condition. As the nonlinearity is increased further, the initial domain can move and spatial structures with a characteristic wavelength appear in the patterns (see figure 4 (top)). These eventually dominate at higher nonlinearity (see figures 4 (bottom) and 5). As the nonlinearity is increased further, this period-doubling sequence loses its stability to a sequence exhibiting intermittency via pattern competition. This forms the subject of a subsequent section.

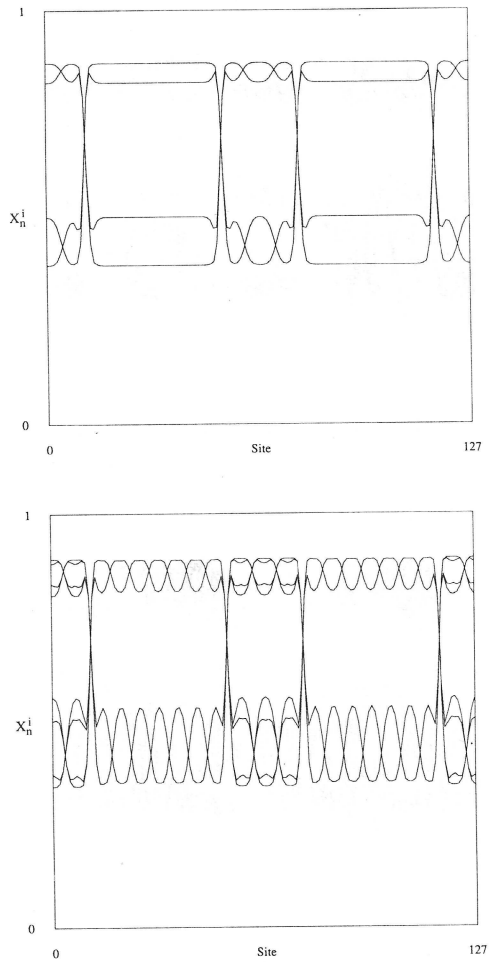

Figure 2. Amplitude versus space graphs for the future-coupled logistic lattice. The systems started from a single sine wave initial condition: $x^i = 0.5 + .4\ sin\,(2\pi iN^{-1})$. Boundary conditions are periodic and the coupling strength is $\varepsilon = 0.2$. The nonlinearity of the local dynamics increases in this and the following sequence of three figures. Above the amplitudes x^i are overlapped for 32 time steps after the transients have died out. Here r = 3.5 (top) and r = 3.57 (bottom). The attractor's period is 4 in the former and 8 in latter.

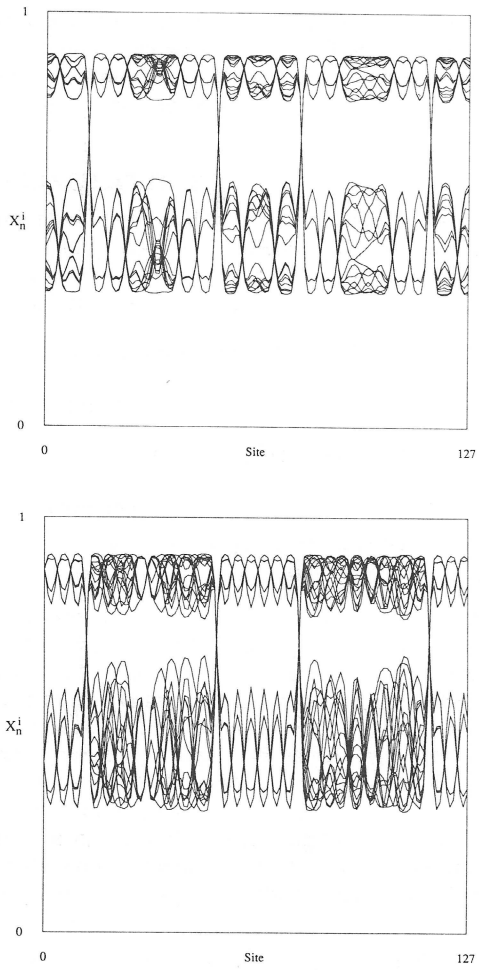

Figure 3. Larger nonlinearity: r = 3.6 (top) and r = 3.65 (bottom); These and the following figures illustrate chaotic domains whose periodicities decrease via domain-merging. Details as in the preceding figure.

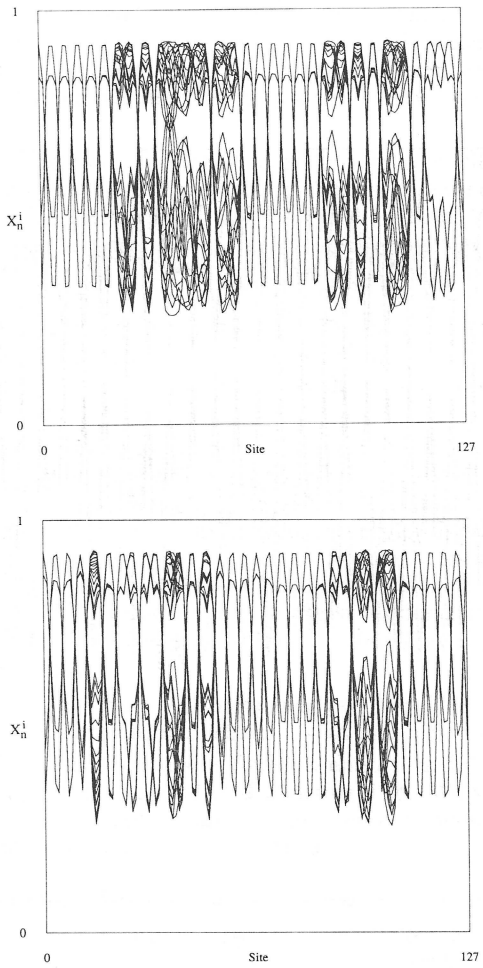

Figure 4. Larger nonlinearity: r = 3.7 (top) and r = 3.71 (bottom); In the top figure the amplitudes x^i are overlapped for 16 time steps after the transients have died out. In the bottom the overlap is 32 time steps.

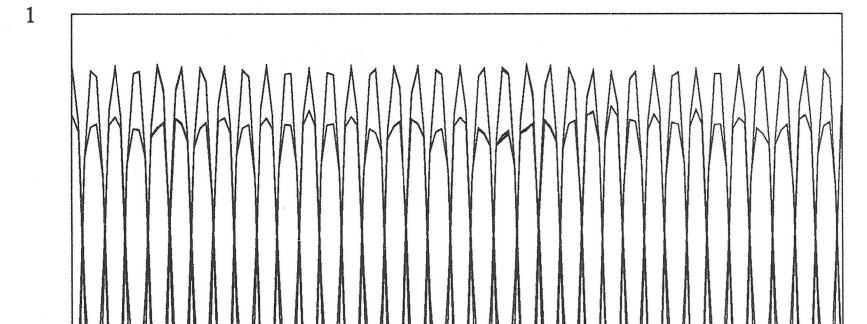

Figure 5. The nonlinearity is r = 3.75. Here the amplitudes x^i are overlapped for 16 time steps after the transients have died out.

The overall period-doubling sequence is conveniently pictured with two types of bifurcation diagram: site histogram and spatial pattern. The former is shown in figure 6, where the familiar period-doubling structure envelopes the range of sites values from the periodic behavior at the top to the chaotic at the bottom. The control parameter varies from r = 2.9 to r = 4.0, respectively. At each of 256 parameter increments in this range the probability in 256 interval bins is gray-scaled, with black indicating highest probability.

Sites in the domains' interiors contribute to the high probability along curves that follow the isolated map period-doubling structure. The appearance of kinks in the spatial structure beyond the transition to period two gives rise to the cross-hatching inside the envelope. Note that each of these kink-curves radiates from where the period one orbit goes unstable: $r = 3, x^i = \frac{2}{3}$. Much of the kink cross-hatching disappears above the period two superstable parameter* $r_{super} \simeq 1 + \sqrt{5}$. This is due to the consequent change in the approach of individual site initial conditions to the period two cycle below and above the superstable transition. Below, the approach is from one side; above, it is from both sides of the orbit.

The overall transition to spatially complex structures is also mirrored in the spatial pattern bifurcation diagram of figure 7. It illustrates how the spatial structure is changing through the same range of parameters. At each value of the parameter, the pattern is shown in gray scale after 100 iterations from the same single-sine-wave initial condition. Thus, each horizontal line is a snapshot of the pattern at that time and does not indicate asymptotic behavior. Nonetheless, the change in approach to the final pattern below and above r_{super} is clear with the disappearance of the small domains at the top and their associated kinks. Also, the complex patterns illustrate how little obvious structure is left above the transition to chaos.

With regard to both figures, at finite coupling the dominant period-doubling behavior quickly gives way to chaotic behavior, with higher-period cycles washed out. This occurs in much the same manner as found in noisy period doubling systems,[56] so that the couping strength acts as a kind of disordering field. We should note, however, that in other regimes the coupling strength can serve to induce regular behavior. Examples of the latter follow in subsequent sections.

3.1. Dependence of Domain Behavior on Domain Size

One noteworthy aspect of spatially-extended systems is the possibility of a *spatial bifurcation,* in which the system size (number of sites) is varied. This is somewhat akin to finite-size scaling techniques used to study critical phenomena. With finite-size scaling the assumption is typically that there is a smooth change in behavior; whereas here we shall show that there can be sudden changes. A spatial bifurcation results in a symmetry breaking of a domain's translation invariance via the appearance of new subdomains and kinks. Other spatial invariances might also be broken. Even if the local dynamics itself is homogeneous, the local behavior can differ from site to site. This already appears in

*For the isolated map $r_{super} = 1 + \sqrt{5}$. With the future-Laplacian coupling used in this example the domains' stability is governed by the isolated map. Deviations from this occur near the domain walls, and so this estimate of the superstable parameter value for the lattice is only approximate.

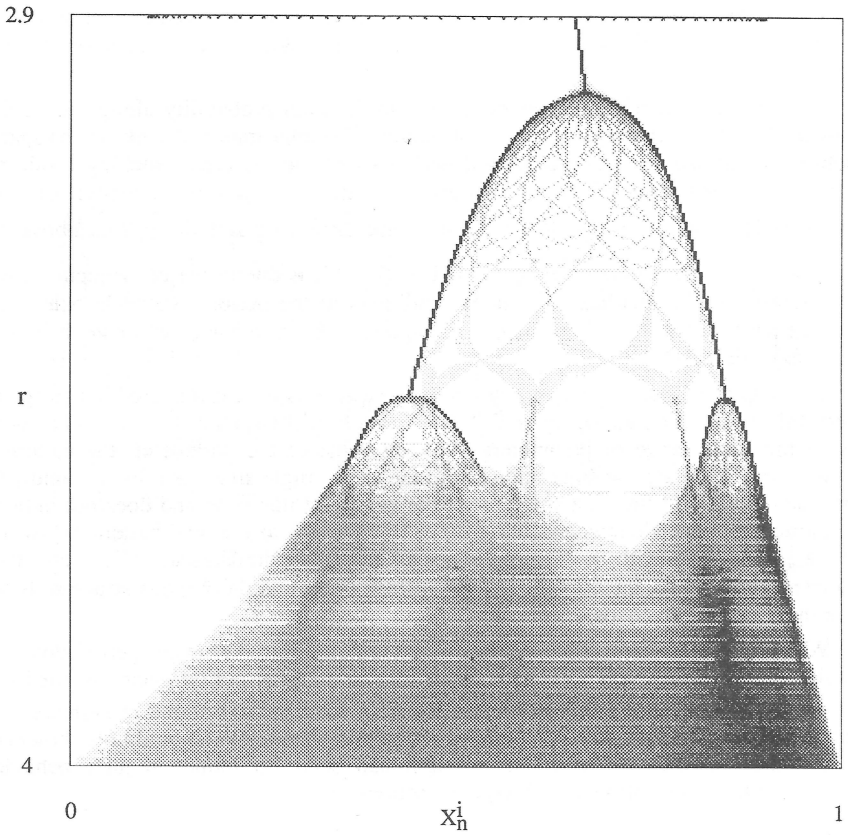

Figure 6. Site histogram bifurcation diagram through a period-doubling sequence. The nonlinearity parameter is incremented 256 times in the range of r = 2.9 to r = 4.0. The coupling strength was fixed at ε = .2. Logarithm (base 2) of the probability is shown in gray scale, with black indicating highest probability. This is computed with a frequency histogram of site values in 256 site-value bins over 400 iterations after 100 transient iterations. The lattice contained 128 sites. The single spatial sine wave initial condition is shown at the top.

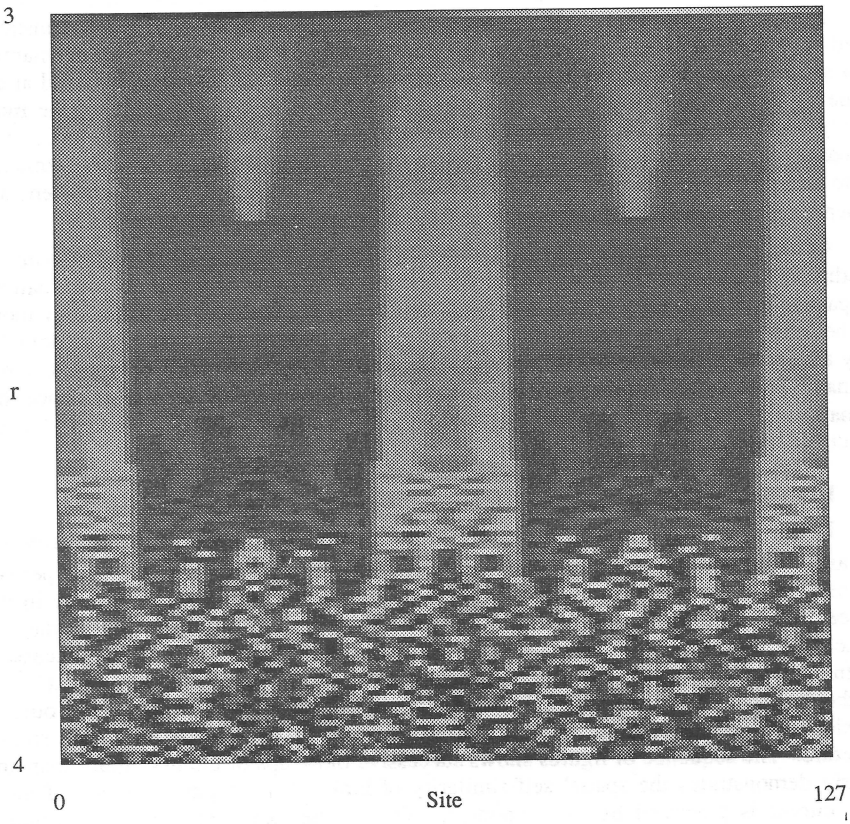

Figure 7. Pattern bifurcation diagram through a period-doubling cascade to chaos. At each of 128 parameter increments from r = 3.0 to r = 4.0, the lattice pattern is shown gray-scaled after 100 transient iterations. The coupling strength, as before, is fixed at $\varepsilon = .2$ and there are 128 sites.

the period-doubling case (figure 3 (top)) where domains of different size have different periodicities. In figure 3 (top) some domains have a noisy periodicity of 8, while other domains appear chaotic. (For other examples see also references (35) and (57)). We now study this in more detail.

A geometric description of this symmetry breaking can be developed as follows. As already noted, the walls or kinks pass through saddle points which are separatrices of two out-of-phase regions. That is, the kinks connect two domains through locally unstable fixed or periodic points. The dynamics in a domain can be approximated by the dynamics of a small system with fixed boundary conditions at both ends; specifically, fixed at the value of the unstable fixed or 2^k-periodic points. The narrower the domain, the more highly constrained the dynamics and so the simpler the behavior. Thus, as a function of domain size, we have a bifurcation sequence to more complex behavior and eventually on to chaos at some critical size $N_c = N_c(r, \varepsilon)$. Figures 8 through 10 show the system size dependence of domain behavior.

Of course, the replacement of a domain by a finite system with fixed boundary conditions is an approximation. The simplification is that one assumes no perturbations propagate from domain to domain through the walls. In principal, the kinks may move or the sites may not lie exactly on the locally unstable periodic orbits and so domains may affect one another. Nonetheless, the approximation appears valid. The coexistence of many domains of different periods, as in figure 3 (top), can be taken as evidence that domain independence is a good approximation even when fairly complex domain structures are present.

3.2. Kink Self-similarity

Period-doubling in low-dimensional systems exhibits temporal self-similarity via the associated attractor's scaling structure, as formulated by Feigenbaum.[58] The period-doubling of domains in the logistic lattice also introduces spatial self-similarity in the lattice field. Figures 11 and 12 illustrate this with spatial return maps where the site values are *spatially reconstructed* by plotting points (x^i, x^{i+1}). With successive magnification more detail is revealed on finer scales. The domains in which $x^i = x^{i+1}$ lie on the diagonal. They are "local" fixed points in the spatial return maps. The outside envelope of deviations from the diagonal corresponds to the loci of the kinks' spatial structure. The sequence of figures shows successive blow-ups of the first return map and clearly demonstrates the spatial self-similarity of kinks. The similarity scaling of these kink curves is governed by two exponents. One is the exponent α in Feigenbaum's notation, which determines the scaling along the $x^i = x^{i+1}$ line while the other corresponds to the scaling for the deviation from the line $x^i = x^{i+1}$. The latter exponent is given by the instability of Feigenbaum's functional fixed point against perturbation in the coupling term. Though we do not discuss the numerical estimate for the exponent, it is obtained in a similar way with the scaling of noisy period-doubling[59, 60] or torus doubling.[61, 62, 63] (See reference (64) for further discussion.)

4. SPATIAL MODE INSTABILITY: THE TRANSITION FROM TORUS TO CHAOS

In nonlinear systems, quasiperiodic states are commonly observed. Many dynamical systems exhibit a bifurcation sequence to successively more complex behavior

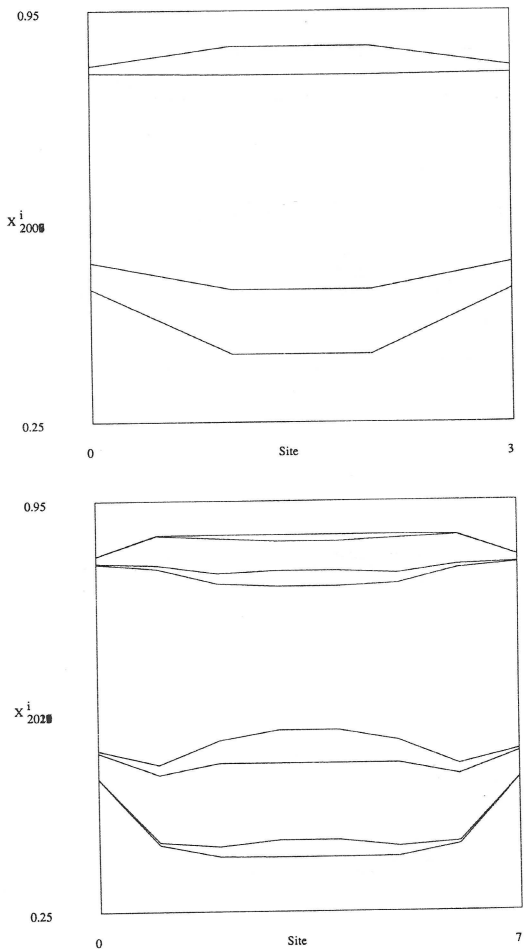

Figure 8. Space-amplitude plots for the future-coupled logistic lattice demonstrate the dependence of temporal period on the size N of the lattice at fixed parameter values. In this and the following two figures. N ranges from 4 to 64 by factors of two; the observed periods increase from 4 to 8, 16, 16, and then finally to 32, respectively. Above N = 4 (top) and N = 8 (bottom) are shown. The site amplitudes x^i are plotted after transients have died out. The boundary conditions are fixed at "sites" i = -1 and i = N to a value of $x^* = 1-r^{-1}$, the fixed point of the isolated logistic map. In all figures the parameters are fixed at r = 3.57 and ε = .2. The initial condition was $x = x^* + .01\ sin(\pi i N^{-1})$.

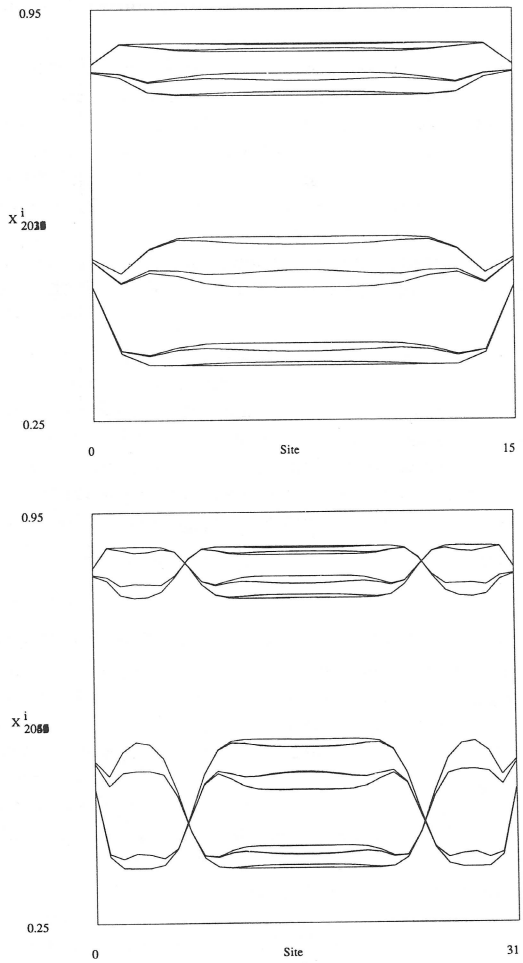

Figure 9. Details as in the previous figure, except there are 16 (top) and 32 (bottom) site lattices exhibiting period 16 cycles.

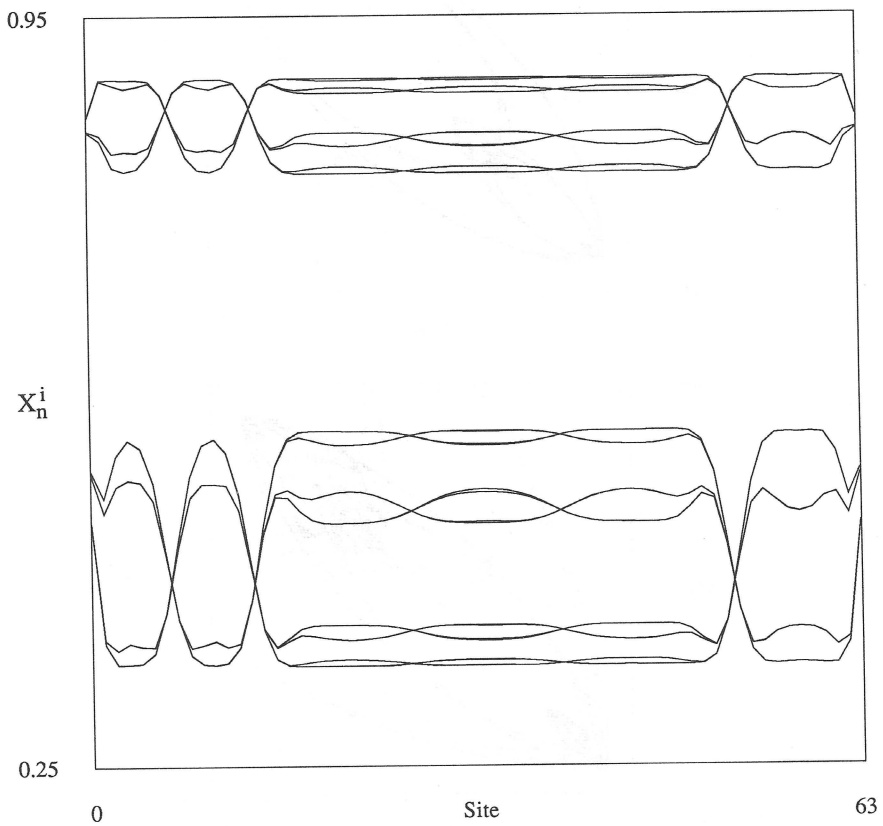

Figure 10. Details as in previous figures, except there are 64 site lattices exhibiting a period 32 cycle.

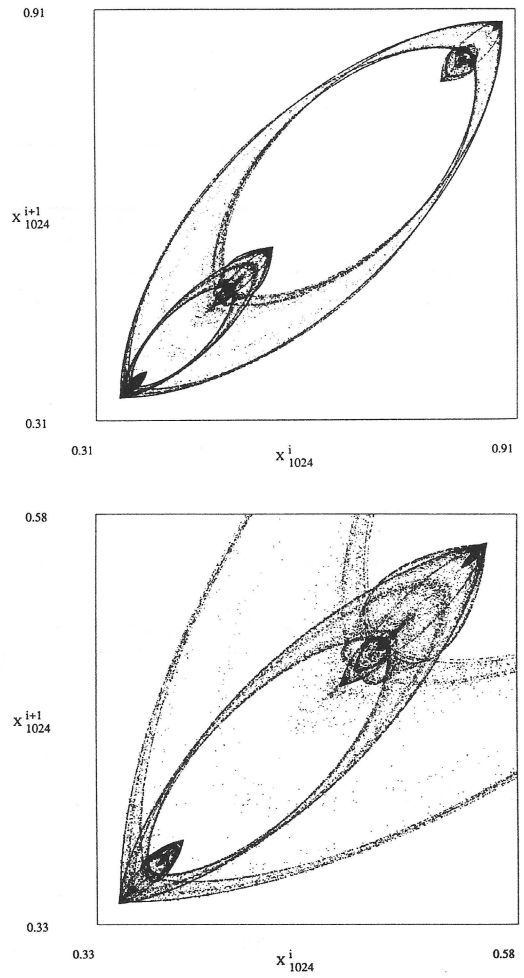

Figure 11. ''Snapshot'' spatial return maps for the future coupled logistic lattice with r = 3.56995 and $\varepsilon = .3$. The plot of x^i versus x^{i+1} is shown for a lattice with 65536 sites. 1024 iterations were performed to allow for the transients to relax. The spatially random initial condition generated many kinks. A uniformly distributed random variable with mean .5 and standard deviation .2 was sampled for the initial condition. This and the next figure are successive blow ups to show the self-similarity.

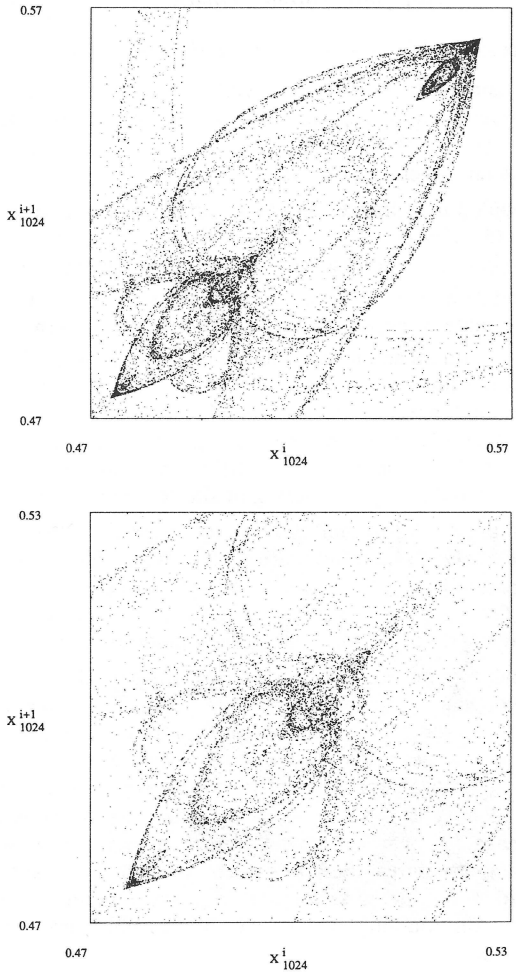

Figure 12. Further magnifications; details as in the preceding figure.

that follows the path

$$\textit{limit cycle } S^1 \rightarrow \textbf{Hopf bifurcation} \rightarrow \textit{quasiperiodic state } T^2$$

$$\rightarrow \textbf{devil's staircase lockings} \rightarrow \textit{chaos or high-dimensional torus } T^k$$

In lattice systems this quasiperiodic route is observed frequently, accompanied by spatial instability of some characteristic wavelength. Unlike low-dimensional systems, the temporal oscillation induces spatial quasiperiodicity in the lattice field. In this section, we will discuss in some detail several examples.

A large class of coupled map lattices shows an anti-correlated *zigzag* instability in which the uniform field $x^i = constant$ loses stability to a state of the form $x^i = constant + (-1)^i \cdot amplitude$. The resulting pattern has a spatial wavelength of two sites and so is reminiscent of an anti-ferromagnetic spin system.[1,53] If the lattice is two-dimensional, the zigzag pattern appears as a checkerboard pattern. This has been investigated by the present authors and independently reported by Kapral.[65] The structure is also frequently seen in the linear coupling model over a wide parameter range and in the future coupling model with small coupling strength. With future coupling, the zigzag instability is suppressed, especially with strong coupling, since neighboring sites are kept in-phase by their future or "pre"-iteration. The diffusive coupling then maintains the sites' phase coherence by spatial low-pass filtering of site-to-site differences.

The development of the zigzag instability is shown in figure 13 for linear Laplacian coupling, where the state evolves in a temporal period-2 cycle. Here we note that kinks can exist, as seen in figure 13 (top). The width of a kink increases as the parameter approaches the onset of the zigzag structure. A space-time diagram (figure 13 (bottom)) shows the evolution of zigzag domains and kinks from a random initial pattern.

Approximately speaking, the kinks connect two anti-correlated zigzag domains through the unstable homogeneous solution, a saddle point. The latter is given by the unstable periodic orbit of the local dynamics which, in this case, is a fixed point. At a kink position, the site values x^i pass close to the periodic saddle with $x^i = constant$. The spatial return map of x_n^{i+1} versus x_n^i for this situation is shown in figure 14. Sites in the kinks pass close to the identity $x^{i+1} = x^i$. Sites in the zigzag domains lie far off the identity. The zigzag kinks lie near the spatial return map identity, whereas in the preceding domain-doubling structures, the kinks were associated with spatial return map states away from the identity. Here, kinks are in-phase structures separating anti-correlated domains; in domain-doubling, they connect out-of-phase domains by smoothly relaxing the phase difference.

As the nonlinearity is increased, a torus appears through a Hopf bifurcation. The quasiperiodicity is easily observed again using spatial return maps. We shall discuss a bifurcation sequence from a torus attractor to chaos for the additive linear coupling model first introduced

$$x_{n+1}^i = f(x_n^i) + \frac{\varepsilon}{2}(x_n^{i+1} + x_n^{i-1}) .$$

Figure 15 gives an amplitude plot that shows a single zigzag domain with a long wavelength modulation. Figure 16 presents a mosaic of space-time return maps for this, where x_{n+k}^{i+j} versus x_n^i (j, k = {0, 1, 2, 3}) is shown for N-j sites and 32 time steps. These

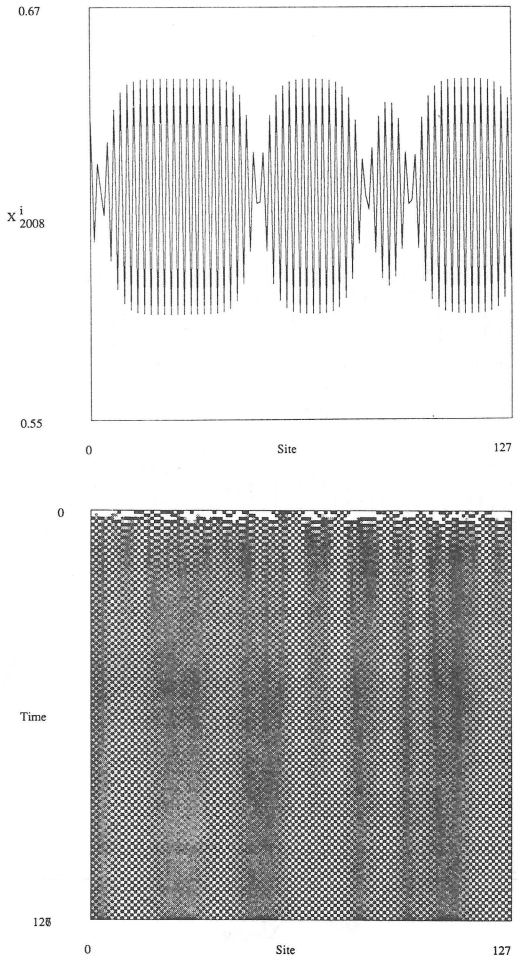

Figure 13. (top) Snapshot of pattern for the linear Laplacian coupled logistic lattice with $r = 2.61$ and $\varepsilon = .1$ after the transients have died out. A uniformly distributed random initial condition of moderate amplitude was used. (bottom) Space-time diagram for this system. The temporal period of the attractor is 2, as is the dominant spatial period.

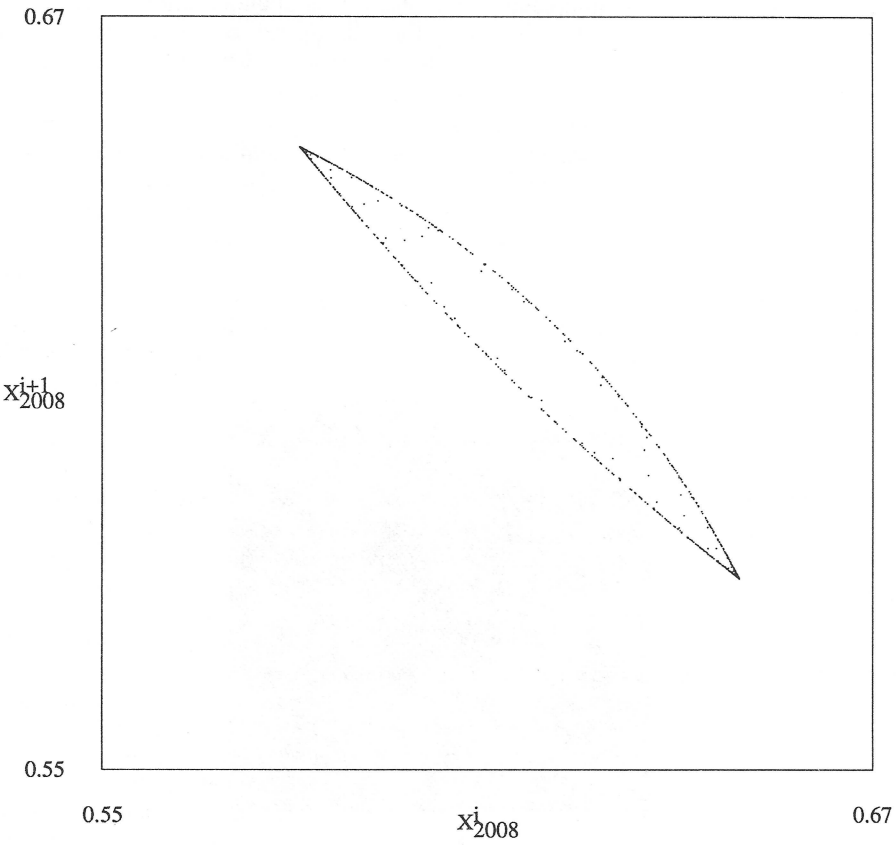

Figure 14. Spatial return map in the zigzag regime when the pattern contains several zigzag domains and their kinks. Details as in the preceding figure, except that the lattice contains 2048 sites.

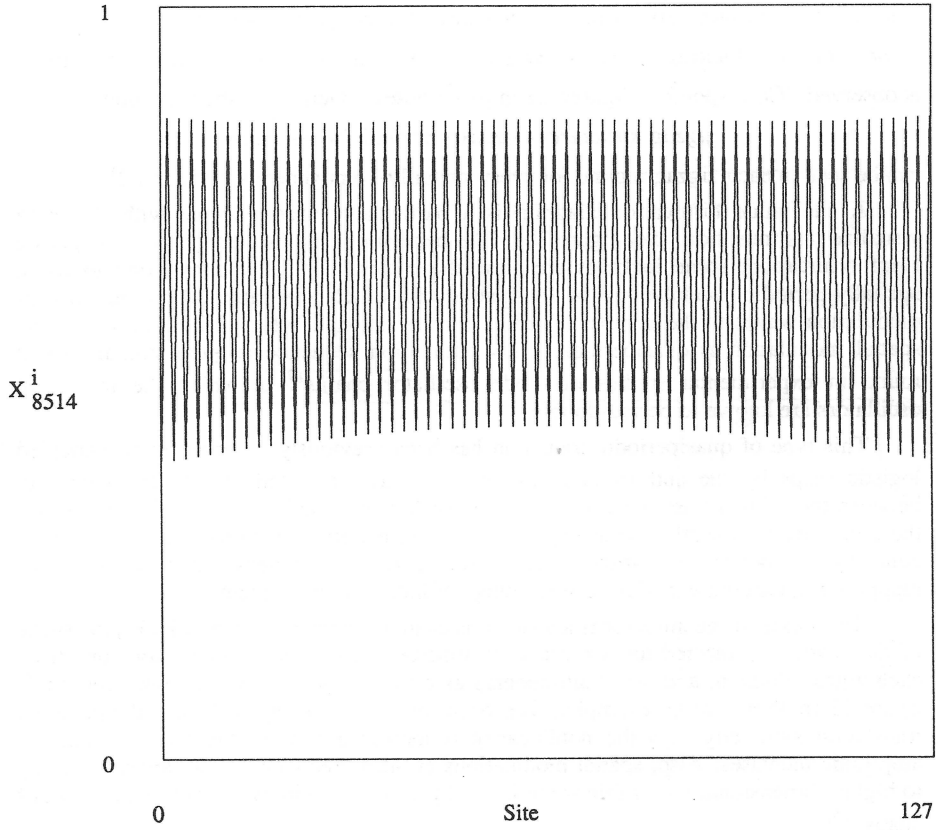

Figure 15. Snapshot of the coupled logistic lattice with additive linear coupling with r = 3., $\varepsilon = 0.075$, and N = 128, after the transients have died out. Initial condition is a half sine wave with mean 2/3 and amplitude .2.

return maps correspond to projections of the entire state space onto various two-dimensional planes. They clearly demonstrate the existence of a "two-torus". The anti-correlated spatial structure is seen in moving horizontally from figure to figure in the mosaic; the temporal period 2, in moving vertically. The tori alternately lie near the identity in the return maps or near $x_{n+k}^{i+j} = 1 - x_n^i$.

In figures 17 through 19, one portion of the associated torus in the spatial return maps is shown at successive parameter changes. The bifurcation sequence

$$\textit{torus}\ (17t) \rightarrow \textbf{locking}\ (17b) \rightarrow \textit{chaos}\ (18t) \rightarrow \textit{higher complexity chaos}\ (18b\text{–}19)$$

is observed. (Corresponding figures are in parentheses). Generally, the transition

$$\textit{zigzag structure} \rightarrow \textit{quasi–periodicity} \rightarrow \textit{chaos}$$

can be seen in each zigzag regime for every spatially-homogeneous, temporal 2^k-cycle.

A site value bifurcation diagram is a particularly useful device with which to visualize this transition. (See figure 20). The behavior at the first transition undergoes a Hopf bifurcation; some lockings are seen above this. The latter correspond to fixed, spatially-periodic modulations of the pattern in which the ratio of the number of modulation waves to the number of lattice sites is rational. When tori are observed, the spatial modulation is quasiperiodic. This bifurcation sequence is quite similar to that found in experimental studies of diode oscillator chains[17] in which the individual oscillators are known to period-double.

This type of quasiperiodic transition has been previously observed in two coupled logistic maps by the authors and has been variously reported.[66, 67, 68] The similarity between these low-dimensional systems and the lattice behavior is not accidental. When the anti-correlated spatial symmetry of the zigzag pattern is factored out of the lattice equations of motion, the lattice system reduces to a two-dimensional mapping. This mapping is an accurate model for some range of lattice control parameters.

Kinks exist if the attractor is a torus or is chaotic. In the presence of kinks, the shape of the spatially-projected torus reveals the superposition of out-of-phase tori, one from each zigzag domain, and the result appears as a folded torus. (See the lower portion fo figure 21 (bottom) for an example.) The occurrence of kinks again breaks the pattern's translation symmetry. As the nonlinearity is increased further, the torus modulation amplitude increases. Also, spatial modulations at other frequencies may appear, leading to higher-dimensional tori within some limited parameter regimes just below the onset of chaos.[1, 53]

If the coupling is weak and the nonlinearity large in the Laplacian future coupled logistic lattice, the zigzag instability is also seen. Figures 21 and 22 show spatial return maps for this. One again finds quasiperiodically modulated structures with kinks (figure 21 (bottom)), lockings (figure 22 (top)), and chaos with remnant zigzag structures (figure 22 (bottom)).

We have described a few aspects of the patterns and dynamics found in the zigzag regime. Before concluding this section, we summarize the characteristic features:

(i) Spatial quasiperiodicity: Quasiperiodic behavior in time induces spatial quasiperiodicity.

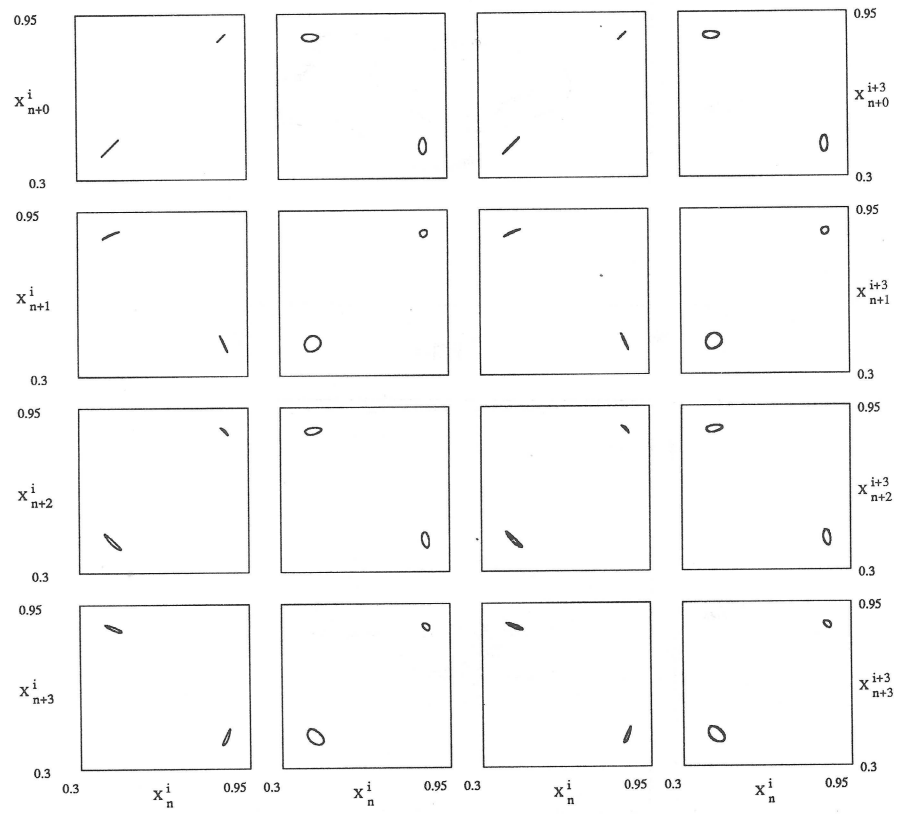

Figure 16. Space-time return map mosaic for the pattern in the preceding figure. The mosaic gives the plots for (x_n^i, x_{n+k}^{i+j}) for j, k = {0, 1, 2, 3}. The plots are overlaid for 32 time steps for N-j sites.

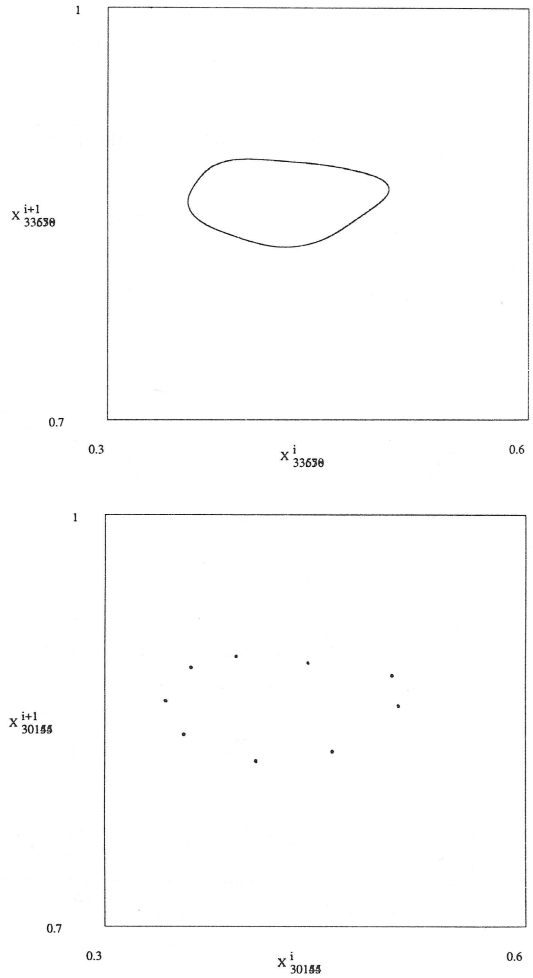

Figure 17. Bifurcation sequence of spatial return maps for the same model as in the previous figure, focusing on just one of the "tori". The plots of (x^i, x^{i+1}) are overlaid for 32 time steps for the entire lattice. The initial condition was a half sine wave with mean .7 and amplitude .2. The coupling strength is varied systematically from figure to figure for $\varepsilon \in [.08,.095]$. Above, $\varepsilon = .08$ (top) and $\varepsilon = .083$ (bottom).

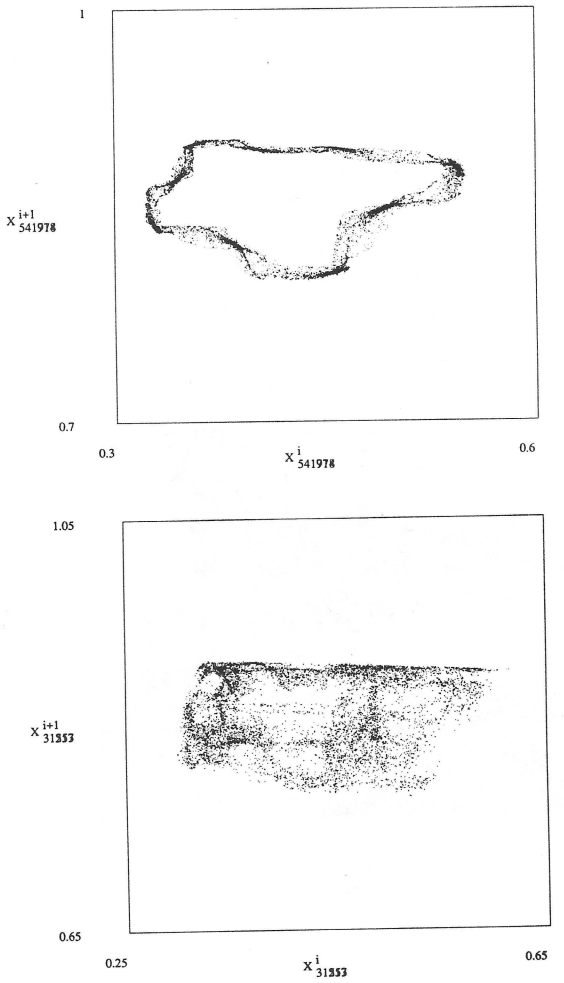

Figure 18. Details as in the preceding figure. Here $\varepsilon = .087$ (top) and $\varepsilon = .09$ (bottom).

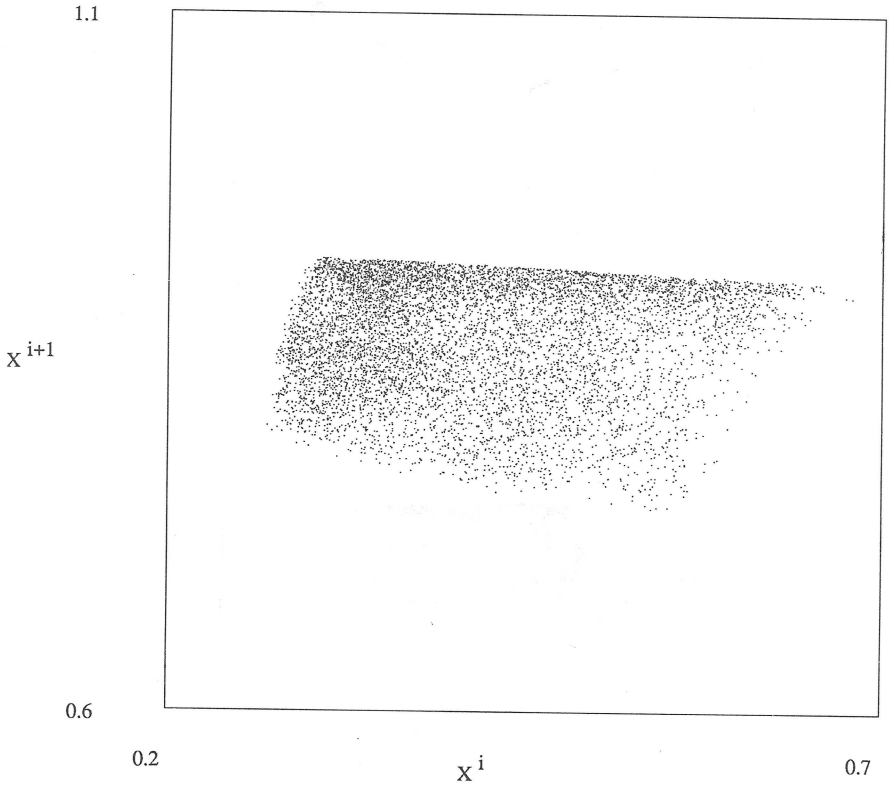

Figure 19. Details as in the preceding figures, except $\varepsilon = .095$.

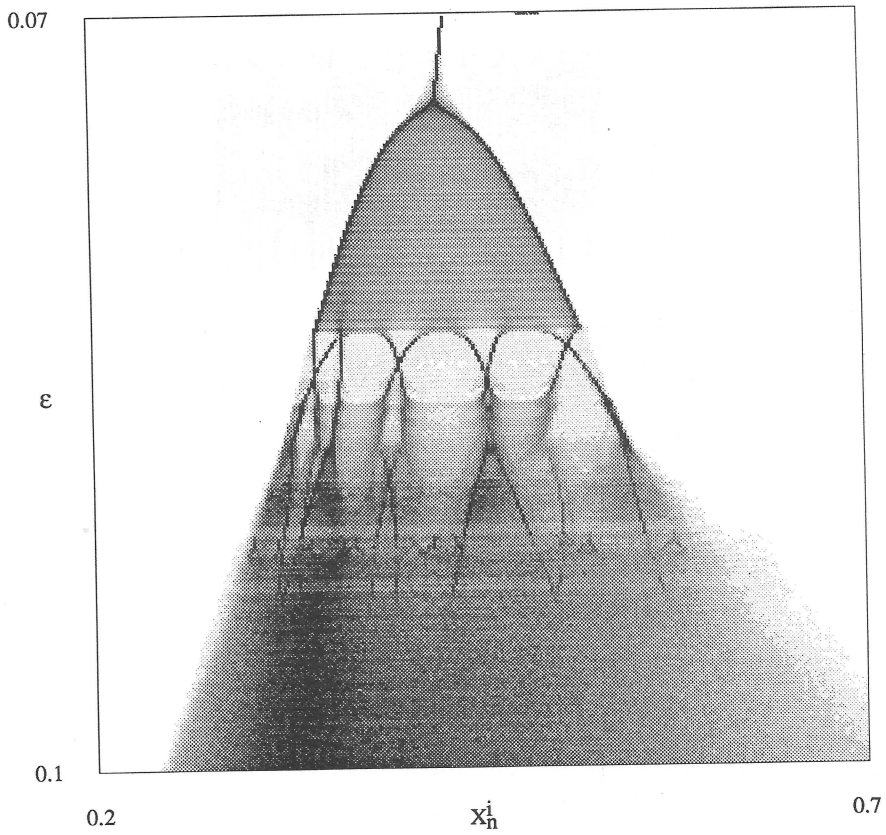

Figure 20. Site bifurcation diagram for the transition from the zigzag pattern to chaos through quasiperiodicity, focusing on the same "tori" as in the preceding figures. The vertical axis covers the same range of coupling parameter as in the previous sequence. ε varies from .07 to .1, with fixed nonlinearity r = 3. As before, the logarithm of the probability is plotted in gray scale. Here, there are 256 increments in ε and 256 histogram bins. Estimates of the bins' probability were collected from 400 iterations of a 128 site lattice, after 100 transient iterations.

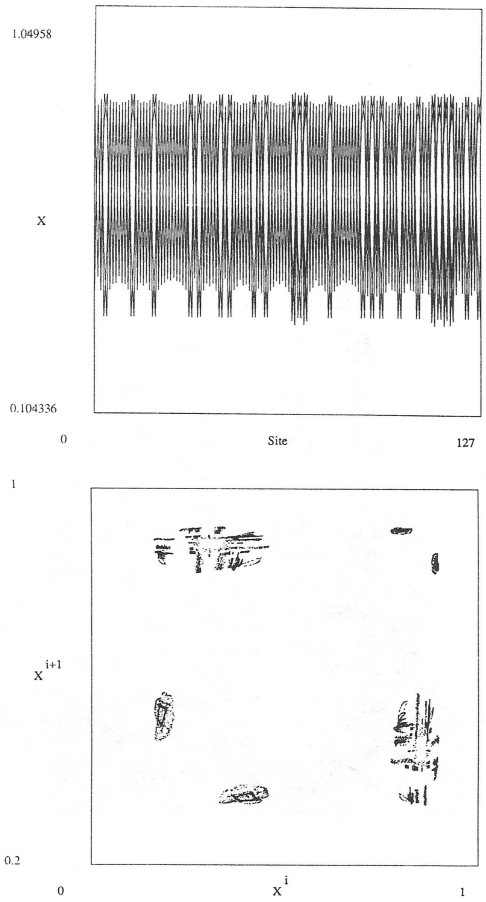

Figure 21. (top) Space-amplitude plot for the Laplacian future-coupled logistic lattice in the zigzag regime with many kinks (r = 3.78, $\varepsilon = .1$). Amplitudes x^i are overlaid for 2 time steps after the transients have died out. The temporal period of the attractor is 2. N = 128 and $\varepsilon = 0.1$. A random initial condition was used. The lower figure and the following figure present spatial return maps for the same model using the same initial condition. The nonlinearity r is varied with fixed $\varepsilon = .1$ in the transition regime from torus to chaos. Points (x^i, x^{i+1}) are plotted for 600 time steps after transient iterations. The spatial return map plots are overlaid for N-1 lattice points. The parameter for the lower figure is r = 3.8.

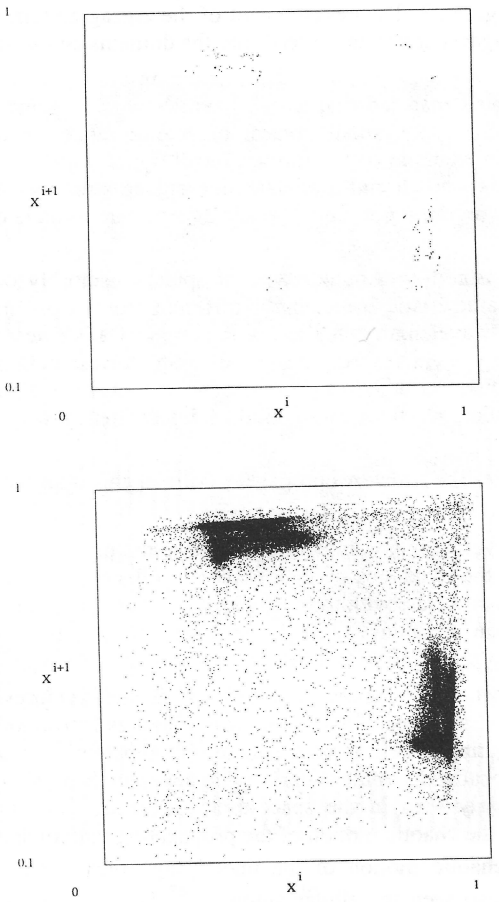

Figure 22. The parameter varied in these is r = 3.81 (top) and r = 3.91 (bottom). Details as in the lower half of the preceding figure.

(ii) Zigzag structure formation: Starting from a homogeneous state with small perturbations, the evolution from the homogeneous state to the zigzag pattern appears as in figure 23. The development of the zigzag pattern starts at the domain walls and propagates at constant speed into the domains and so destroys them.

(iii) Universality of zigzag structures: The zigzag instability can be seen in a wide variety of coupled map lattices, as we have shown. In some lattices, the zigzag structure is limited to a small control parameter range; in others, it is readily observed. As an example of the former, recall figure 14 where the pattern's large-scale structure is smooth and modulates the zigzag structure. More commonly, in large parameter regimes, one finds the zigzag structure modulated quasiperiodically or chaotically.

(iv) Spatial mode instability: Another type of spatial instability occurs where modes appear with characteristic wavelengths different from two. In figure 24 a spatial instability with wavelength ≈ 8 sites, with domain walls every ≈ 4 sites, is shown. As the coupling is increased, the wavelength corresponding to the instability increases. A quasiperiodic route to chaos is seen here also. At the onset of aperiodic behavior, we find a new kind of intermittency which will be described below.

(v) Solitons: particle-like structures propagate, collide, and annihilate. Similar behavior will be discussed shortly in a different lattice.[69]

The latter deserves further comment in regard to the present models, however. One interesting aspect is the dynamics of kink-antikink collisions. If we start from random initial configurations or a state with too many kink-antikink pairs, the kinks and antikinks move around and pair-annihilate until the number of kinks is small. At some small density the kinks stop propagating and a stationary state is attained. (See figure 25 (top).)

In some other parameter regimes, the kinks in zigzag structures propagate as stable particle-like entities. Examples of this are shown in figures 25 (bottom) and 26. Here the profile of the propagating pattern is not periodic, but apparently random and we observe a kind of spatially-localized turbulent burst. The apparent Brownian motion of the kink particles can be clearly seen in the space-time diagrams. The random walk of such particles arises from the chaotic motion of the propagating pattern and, if the nonlinearity is large, from the chaotic motion of the underlying zigzag pattern.[70] The Brownian motion of kinks is also seen in cellular automata.[43] Finally, we note that the diffusive motion is quite similar to the spatial diffusion found for a particle in a periodic potential well,[46] a low-dimensional dynamical system.

These propagating kinks are highly reminiscent of the *turbators* or dislocations observed in low-Reynolds number Couette flow[71] or in large aspect ratio convection flows: localized, stable structures, that appear and propagate, collide and annihilate, ... In two spatial dimensions, Brownian motion of defects is frequently observed in liquid crystal convection and in video feedback.[57] Logistic lattices in analogous regimes should provide useful numerical prototypes for the future studies of such complex ''particles''.

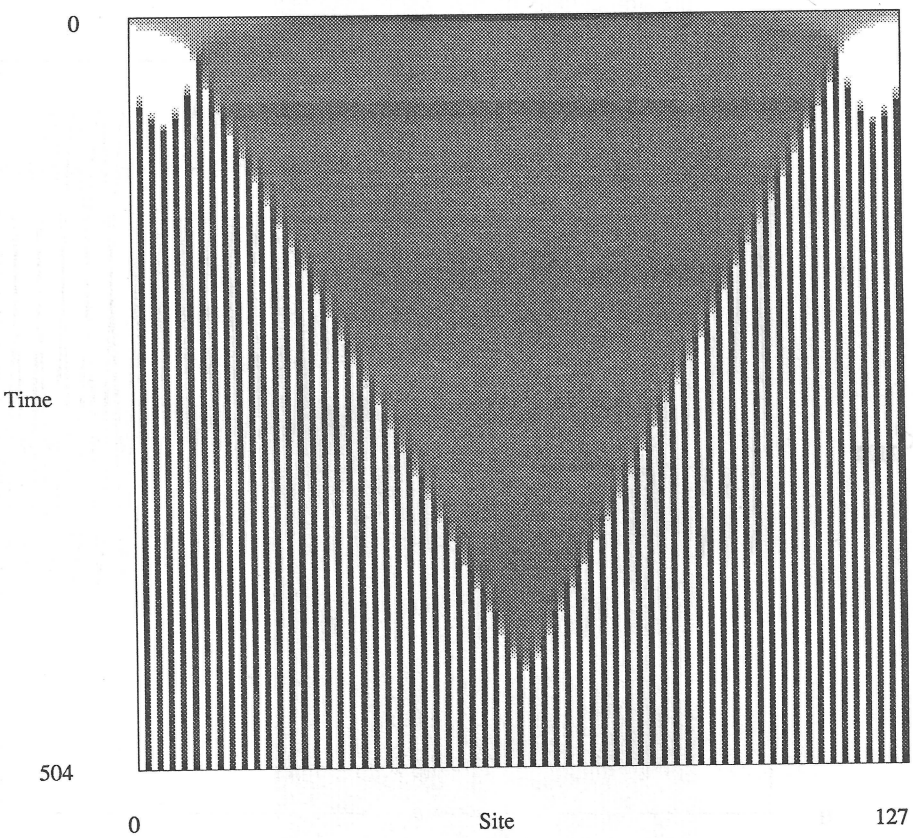

Figure 23. The temporal development of anti-correlated *zigzag* pattern. This shows a space-time diagram with site value in the range of [.63,.93] in gray scale. The lattice system here is the additively-coupled logistic lattice with $r = 3.$, 128 sites, and $\varepsilon = .075$. The initial condition is chosen close to the unstable homogeneous pattern. The pattern is then attracted to a zigzag pattern with some kinks. Every fourth time step is plotted from 0 to $4 \cdot 126$ steps.

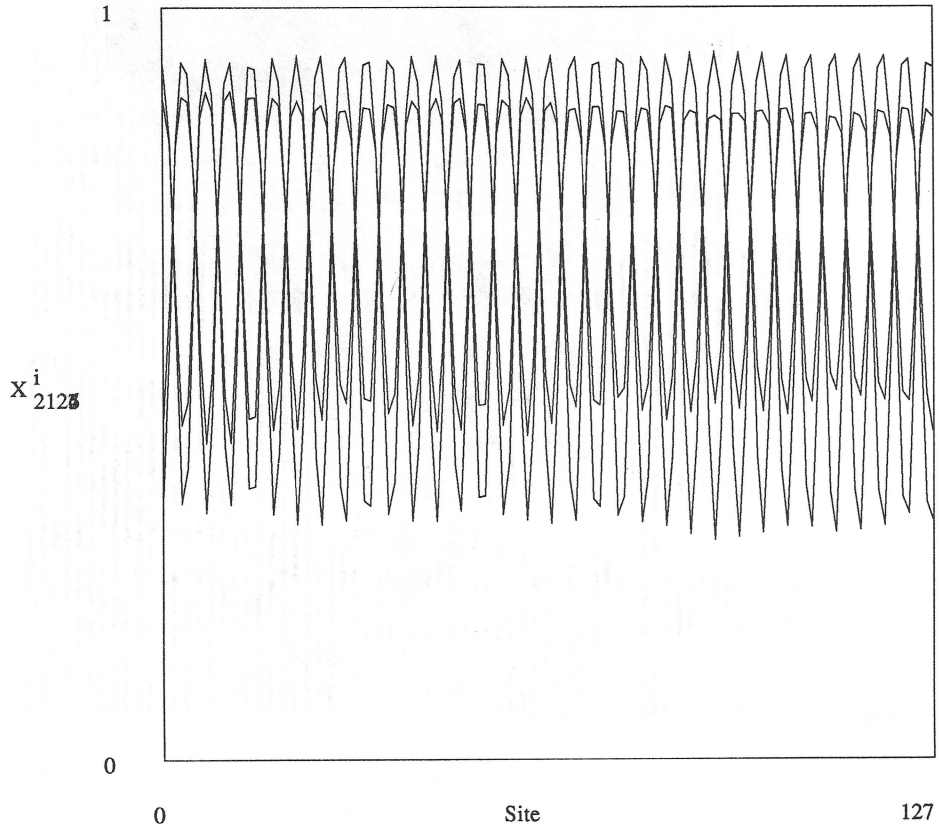

Figure 24. Amplitude-space plots for the Laplacian future-coupled logistic lattice. 4 time steps are overlaid after ~2000 transient steps. Here r = 3.78, ε = .5, and there are 128 lattice sites.

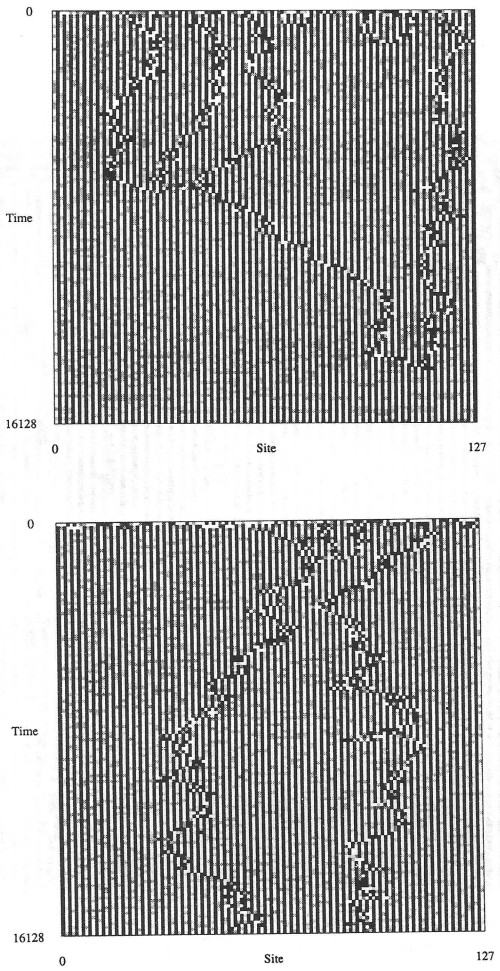

Figure 25. Space-time diagrams with site amplitudes in [.45,.95] represented with light to dark gray scale, respectively. The system is again the Laplacian future-coupled logistic lattice with 128 lattice sites, starting from a random initial condition. Above $r = 3.89$ and $\varepsilon = .1$ (top); $r = 3.91$ and $\varepsilon = .1$ (bottom). In both, the current pattern is plotted every 128 steps from time step 0 to $126 \cdot 128$.

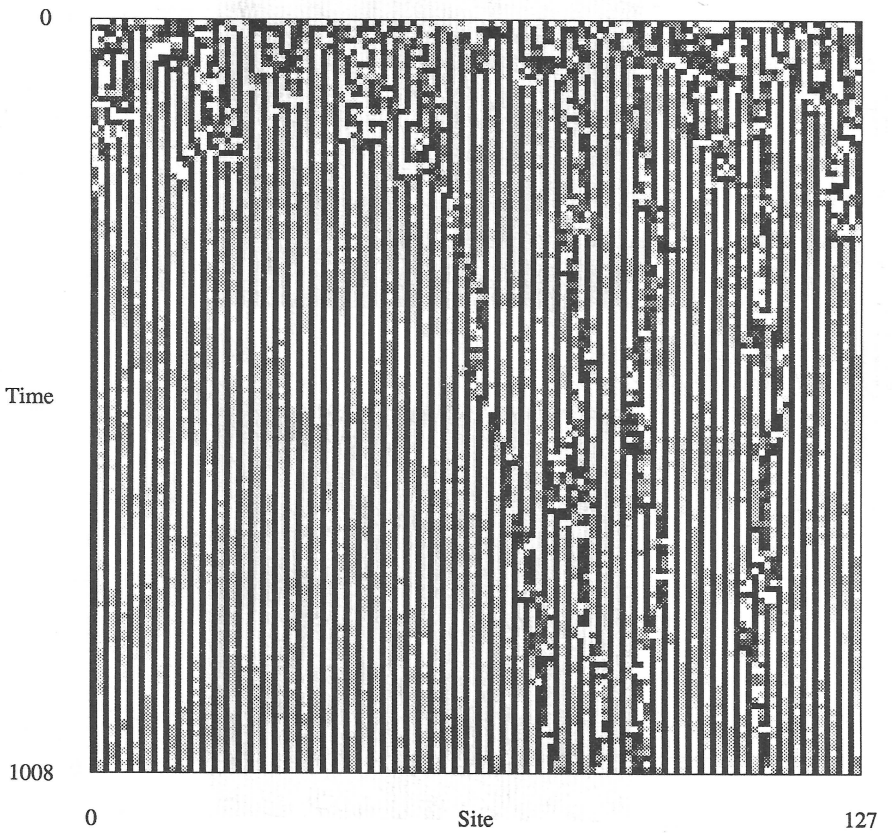

Figure 26. Close up of Brownian kink motion in the zigzag regime. Details as in the bottom portion of the preceding figure. The current pattern is plotted every 8 steps from time step 0 to $8 \cdot 126$.

5. SOLITON TURBULENCE

In the study of phase dynamics the one-dimensional circle map

$$x_{n+1} = f(x_n) = \omega + x_n + k\sin(2\pi x_n)$$

has become a popular prototype as it captures the structure of lockings, critical phenomena of tori collapse, and the statistical properties of the resulting chaotic orbits.[72] In the investigation of spatially-extended phase dynamics, as found in coupled oscillators such as the Josephson junction, the heart and so on, the coupled circle lattice plays a similar role. In this section we consider an example of the Laplacian future-coupled circle lattice described by

$$x^i_{n+1} = (1-\varepsilon) f(x^i_n) + \frac{\varepsilon}{2}\{f(x^{i+1}_n) + f(x^{i-1}_n)\}\ .$$

The frequency parameter ω takes the same value for all lattice positions, as does the nonlinearity k.

The spatial-diffusion coupling compels the independent local oscillations represented by each circle map to synchronize. As a general remark on this system's behavior, it is interesting to note that we have yet to observe quasiperiodic motion with an associated high-dimensional torus attractor. Typically, chaos develops early on as one increases the nonlinearity k.

This transition is analogous to the turbulence scenario proposed by Ruelle and Takens, if we consider the lattice system to be similar to a fluid with isotropic dynamics that exhibits collective quasiperiodic oscillations.[4] This physical interpretation of the Ruelle-Takens scenario is somewhat problematic, however. For example, if the frequency parameter ω is spatially-dependent (at each site i, the local ω^i depends on i), then high dimensional tori are expected.[72] With only three coupled circle maps, the parameter space measure of 3-tori can be large, in contrast to the literal interpretation of the Ruelle-Takens result. Thus, the interpretation of this scenario for spatially-extended systems is unclear at present. We will not pursue this interesting issue any further here.

The spatio-temporal patterns for the circle lattice seem to be similar to those observed in the damped sine-Gordon partial differential equation with external periodic forcing.[51] In some parameter regimes, kinks and anti-kinks pair-annihilate and asymptotically a homogeneous field appears. In others, continuous kink-antikink collisions generate sustained chaotic behavior and the system exhibits aperiodic behavior, complex spatial structures, and a sort of fully-developed turbulence. Between these two extremes, isolated kinks remain and their collisions alone form a sort of billiard-like chaos meandering and colliding in apparently aperiodic spatial trajectories. One observes several different classes of kink-antikink interactions. These regimes are shown in figures 27 through 29 using space-time diagrams of the spatial derivative $|x^{i+1} - x^i|$.

With strong coupling, three different phases, roughly speaking, are found in the following parameter regimes.

(i) $k \leq \dfrac{1.25}{2\pi}$: homogeneous state or periodic behavior (figure 27 (top));

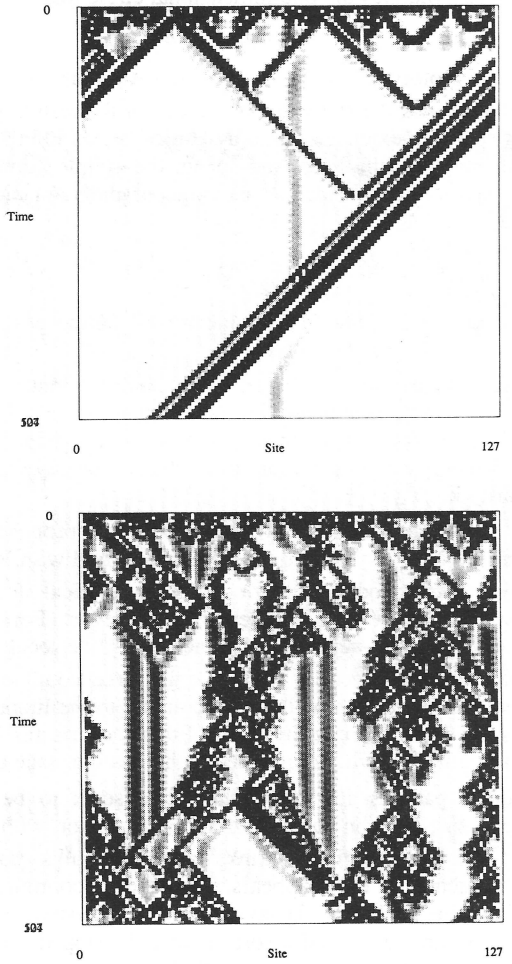

Figure 27. Spatial derivative plots for the future additive-coupled circle lattice in a lattice of 128 sites, with parameters $\varepsilon = .4$, $\omega = .3$, and starting with a random initial condition. The absolute values of spatial first differences $(x^{i+1}-x^i)$ in the range [0,.04] are plotted with gray scale. Every fourth time step is plotted from 0 to $4 \cdot 126$. The nonlinearity parameters above are are $k = .2$ (top) and $k = .203$ (bottom).

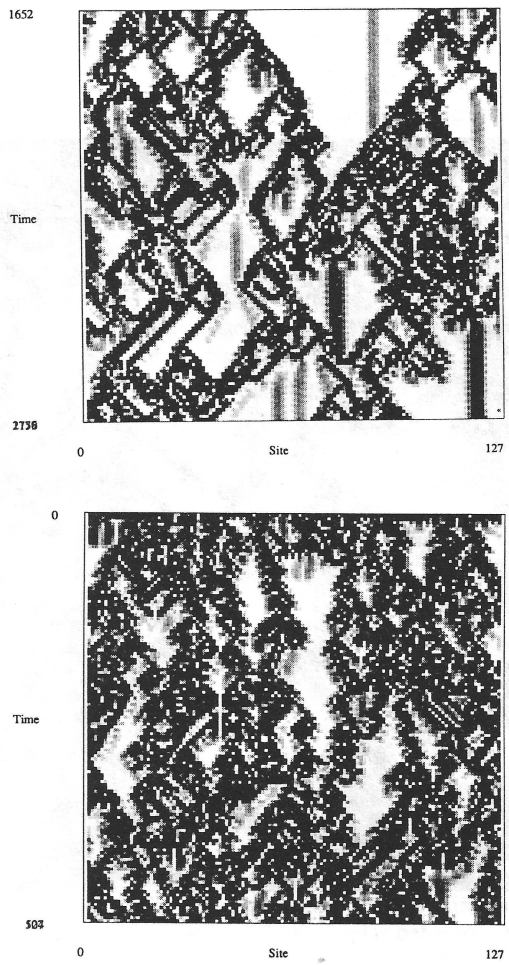

Figure 28. Details as in the preceding figures, except here k = .203 (top) and k = .205 (bottom). The top diagram is the continuation of the bottom one of the preceding figure: time starts at $4 \cdot 413$ and runs for $4 \cdot 126$ steps.

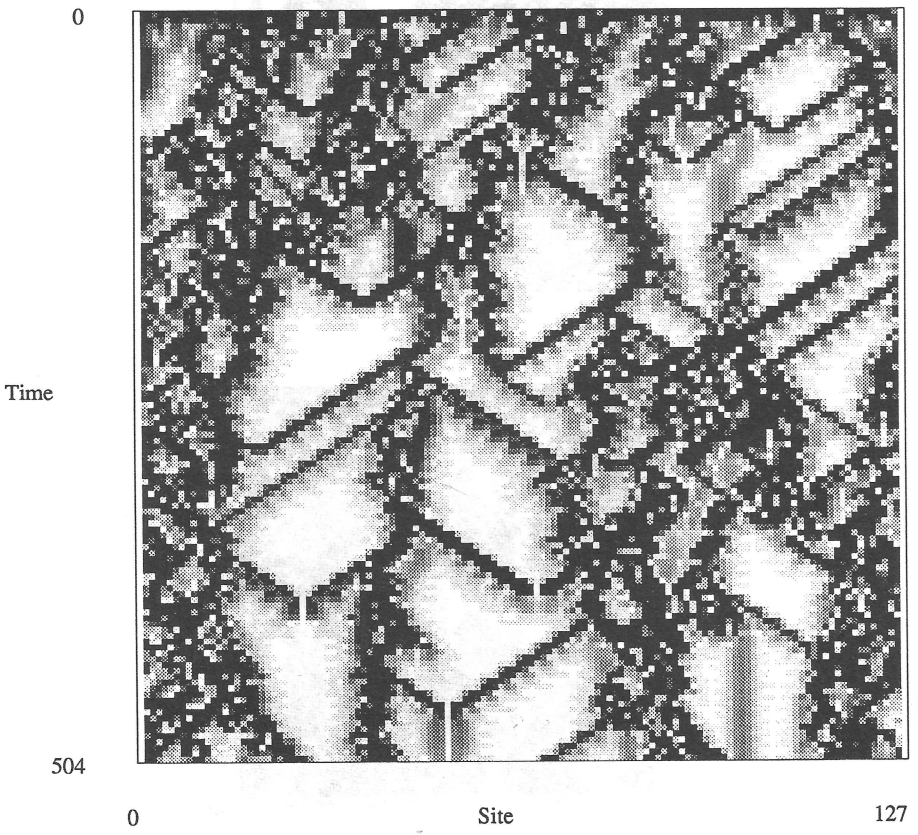

Figure 29. Details as in the preceding figures, except here k = .207. This illustrates the "glider-gun" emission of solitons.

(ii) $\frac{1.25}{2\pi} \leq k \leq \frac{1.3}{2\pi}$: soliton turbulence (figures 27 (bottom) and 28 (top)); and

(iii) $\frac{1.3}{2\pi} \leq k$: fully-developed turbulence (figure 28 (bottom)).

The phenomenon in regime (ii) is called "soliton turbulence" as kink structures remain and the aperiodic behavior is sustained only through their collisions and pair creation and annihilation. Soliton turbulence of this type also has been seen in cellular automata.[73] The soliton turbulence in our system has the following features:

(i) Existence of a nucleus that emits solitons as can be seen in figure 29. Such nuclei are also observed in the two-dimensional Game of Life cellular automaton, where they are called "glider guns",[74] and in a class of one-dimensional automata.[73] One distinguishing feature here, though, is that the emitted soliton can be quite diverse in character, as is readily appreciated in figure 29. Also, the emission of solitons occurs not in a regular manner, but rather in an unpredictable sequence.

(ii) There are many kinds of propagating structures with different velocities as partly seen in figures 27 (bottom) and 29. Consequently, the possible variety of kink-antikink or kink-nucleus interactions is greatly enhanced.

(iii) The interaction depends sensitively on the phase, velocity, and pattern of colliding kinks or nuclei. The turbulent aspect of the system largely originates in this collision instability.

As can be seen in the figures, some aspects of soliton turbulence in these lattice systems are quite similar to class 4 and to soliton turbulence behavior in cellular automata.[73] In the former, long-lived complex transient patterns are frequently observed.[75] Here, this is sometimes observed and leads to $k^{-\nu}$ decay in the spatial power spectra during the transient time.

In parameter space, soliton turbulence is seen just above the transition from homogeneous, or locally oscillating, patterns to developed turbulence. This observation is consistent with the interpretation[42] of class 4 cellular automata behavior as transient phenomena due to the system being close to a bifurcation and marginal stability.

The coupled circle lattice has many features in common with the Sine-Gordon system with damping and external forcing. Soliton turbulence will undoubtedly be observed in this system with extensive and careful simulation studies. For the Hamiltonian version of the Sine-Gordon PDE, similar behavior may be expected since it is seen in preliminary investigations of symplectic lattices.[76]

6. INTERMITTENCY LATTICES

The term "intermittency" originated in fluid dynamics to describe the energy cascade of eddies in turbulence.[77,78,79] Intermittency in low-dimensional dynamical systems, in contrast, is restricted to temporal behavior.[80] It is important to the general problem of fluid turbulence, therefore, to investigate spatio-temporal intermittency in light of this previous work, but with the inclusion of spatial extent. In this section we shall select local dynamics that exhibits Pomeau-Manneville intermittency. This, in concert with spatial diffusion, leads to turbulent regions that intermittently form complex

and laminar structures in space-time.

Another type of spatio-temporal intermittency was recently observed in video feedback experiments[57] and studied in detail numerically by Keeler and Farmer[81] in a "totalistic" logistic lattice.[42] The totalistic lattices are equivalent to strongly future-coupled lattices, as used in the following. Keeler and Farmer hypothesize that this intermittency corresponds to a multiple time-scale dynamics proposed by one of the authors.[82] Similar intermittency appears also to have been observed in the pattern competition in acoustically driven water waves.[83] The topic of pattern competition is briefly described later.

6.1. Spatial Pomeau-Manneville Intermittency

Here we study a coupled system of elements each of which shows Pomeau-Manneville intermittency. We use coupled circle maps, although any local dynamic that is close to intermittent behavior would be appropriate.* The parameters k and ω are chosen so that each isolated circle map has a period 2 locking (k = .2 and ω = .55, for example).†

We have observed the following "phases":

(i) The localized kink regime (small coupling): the coupling is too small for kinks to propagate. Initial kinks separating phase-locked domains remain in their positions. (See figure 30 (top)). This behavior is analogous to the periodic class-2 cellular automata.

(ii) The transition regime: the kinks are unstable and move around, but they are still localized and cannot form global intermittent patterns. (See figure 30 (bottom)). This pattern is similar to the cellular automata class 4.[75] Its occurrence at this intermediate parameter setting is again consistent with the interpretation of class 4 behavior being associated with transient or near-bifurcation behavior by Packard and one of the authors.[42]

(iii) Saturation dynamics (figures 31 and 32 (top)): the burst and laminar regions form trapezium geometric patterns similar to class 3 patterns in cellular automata.[75] In the automata case, regions that "saturate", i.e. all become large at the same time, reset to some low value, and produce laminar regions. The regions then are encroached by inward-propagating disturbances. This occurs in our lattice dynamical system with the additional feature of an initial propagation of localized saturation to larger regions. The distribution of laminar clusters as a function of cluster size obeys an exponential law.

(iv) Fully-developed regime: the burst region is globally extended through all of space-time and it is difficult to discern laminar regions. (See figure 32 (bottom).)

---

*Another example is the logistic map near a periodic window in the chaotic regime. A particularly clear case with this map is found with a slight modification that produces a period 1 window: $f(x) = g(x)$ or $f(x) = 1-g(x)$, if $g(x) = rx(1-x) \leq 1$ or $g(x) > 1$, respectively. This folds the logistic map over so that at $r \approx 5.82843$ there is a period 1 tangent bifurcation and associated intermittency.

†The intermittency for this case but with a different coupling type has been reported by one of the authors.[84]

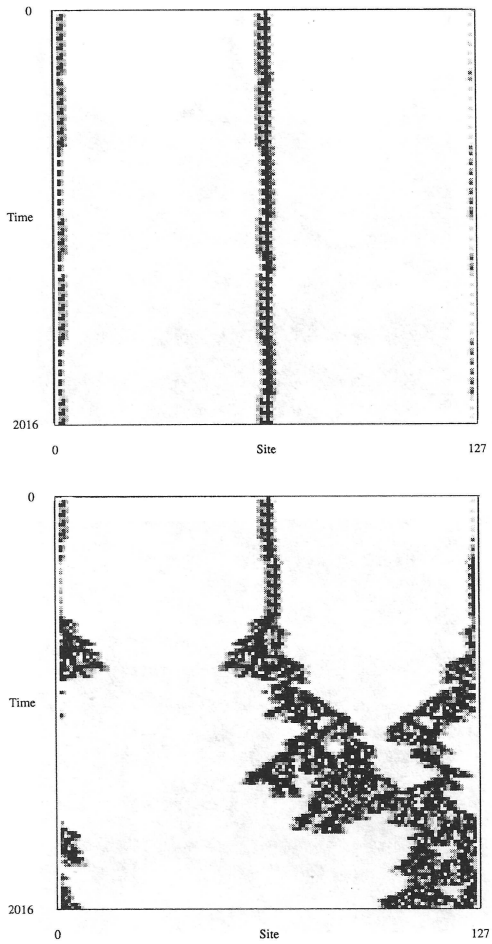

Figure 30. Spatial derivative plots for the future additive-coupled circle lattice with 128 lattice sites and parameters k = .2 and ω = .55. This figure and the next two pairs demonstrate the coupling strength dependence of this intermittency type. In each, the initial condition is a square wave with x = .03 for $0 < i < 2^{-1}N$ and x = .6 for $2^{-1}N < i < N$. When $|x^{i+1} - x^i| > 0.1$, black space-time cells are plotted; differences between 0 and this threshold are shown in gray scale. Each figure in this sequence of 6 starts at step 0 and runs to step $16 \cdot 126$, plotting the lattice pattern every 16 steps. Above the coupling is ε = .22 (top) and ε = .23 (bottom).

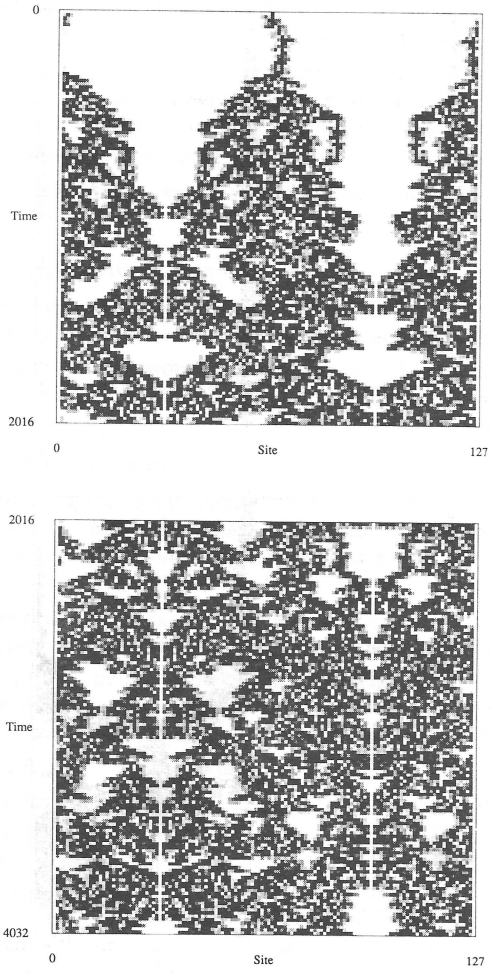

Figure 31. Details as in the preceding figure, except here the coupling strength is $\varepsilon = .25$. The lower figure is a continuation of the top until $2 \cdot 16 \cdot 126$ time steps.

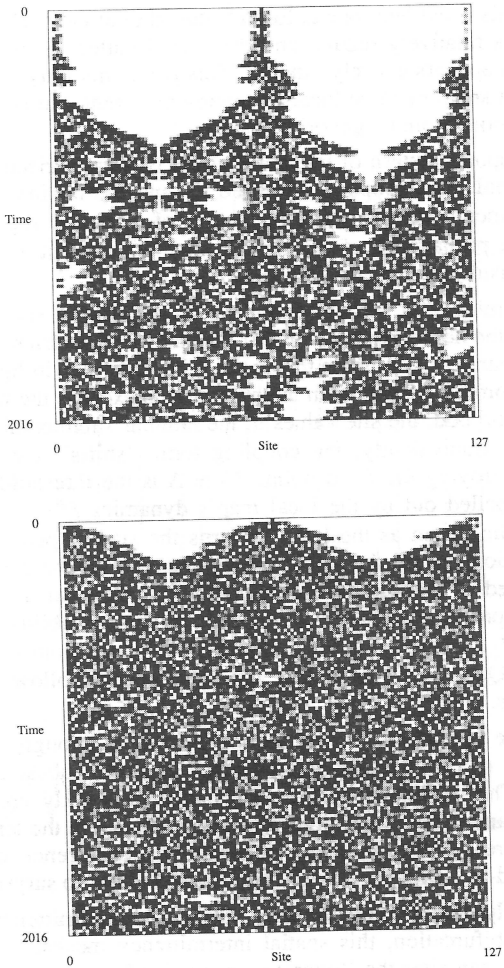

Figure 32. Details as in the preceding figure, except here the coupling strength is $\varepsilon = .27$ (top) and $\varepsilon = .4$ (bottom).

In the saturation regime (iii), an observer following a single site's evolution would observe a temporally-intermittent time series. This is shown in figure 33. Bursting between two channels is evident: one at low x^i, the other at large x^i. When in a channel, the local behavior is relatively regular and the spatial pattern is close to uniform. The time between bursts appears entirely random. This is due not only to the local dynamics being chaotic with a small positive local Lyapunov exponent, but is greatly enhanced by the flow of perturbations from neighboring sites.

The spatio-temporal pattern of laminar clusters is characterized by the existence of two speeds: the initial burst propagation speed v_B and the laminar cluster propagation speed v_L. The former describes the propagation of turbulent regions into a laminar region; the latter, the propagation of the laminar into the turbulent. Estimates of these can be developed by considering the effective local dynamics.

The local dynamics $f^p(x)$ (for period p = 2, in this example) obeys the map shown in figure 34 (top) at the homogeneous region. This temporal return map demonstrates the two intermittency channels. (Compare this to the schematic map in figure 34 (bottom).) If the coupling term from the neighbors in the burst region exceeds the width Δ of the stable fixed point's neighborhood, the site values in the laminar subinterval I_L are repelled out to the burst region. Equivalently, the coupling term "shifts" the map up above the identity, thereby destroying the fixed point. Here Δ is the threshold beyond which the periodic point is repelled out by the local map's dynamics $f^p(x)$. The average v_B is related to this coupling term as the latter governs the size of perturbation of the local state from its evolution toward the stable fixed point x^*. As the coupling is decreased, the propagation speed of the burst decreases until it vanishes at the threshold coupling value. The laminar propagation speed v_L depends on the probability that a chaotic orbit falls on the region I_L, where I_L is the subinterval in which points are attracted to the periodic point x^*. Quantitative estimates for these speeds follow from these simple geometric constraints.

In the example discussed above, we have used a strongly coupled lattice to emphasize that this mechanism for intermittency is quite robust and can appear in different regimes. The authors have previously studied weakly coupled lattices with which one sees "cleaner" demonstrations of this mechanism in the temporal return map. (See, for example, ref. (84)). In these examples the occurrence of intermittency is essentially "designed-in" with very weak coupling and is not so surprising.

Although, closely related to the Pomeau-Manneville intermittency mechanism in its use of near-tangent bifurcation, this spatial intermittency mechanism differs in detail. Here, spatial patterns can alter the "operating region" of the local dynamics, moving it into and out of tangency, and thereby modulating the Pomeau-Manneville intermittency channel. Spatial structure "gates" or strobes the stability of the associated stabilizing fixed point. In the standard Pomeau-Manneville mechanism, the dynamics is time-independent and orbits spend long times in a narrow intermittency channel.

6.2. Intermittency via Pattern Competition

As was already described (recall figure 24), the coupled logistic lattice undergoes an instability at some spatial wavenumber K, developing a stable pattern with that wavenumber. As the nonlinearity is increased, the pattern loses its stability via chaotic

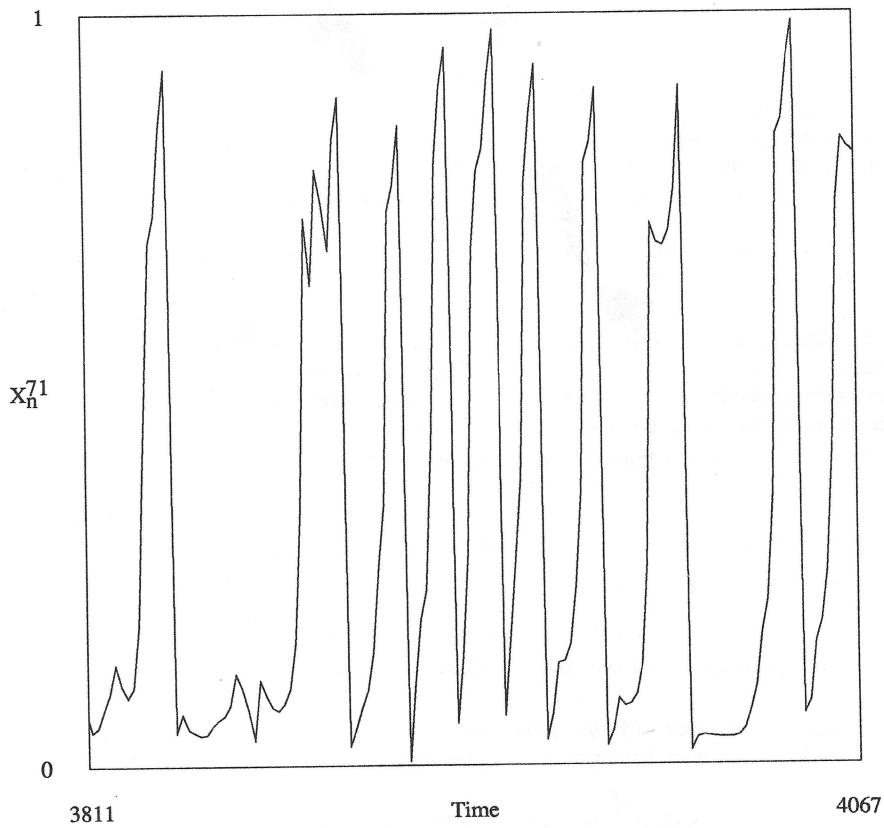

Figure 33. Time series of site values $\{x^{71}\}$ in the saturation intermittency regime for the future additively-coupled circle lattice. Every second iterate is shown for 256 time steps. Bursting between the two intermittency channels is evident. There were 128 sites and the parameters were k = .2 and ω = .55. The lattice started with a uniformly distributed random initial condition with mean .5 and standard deviation .2.

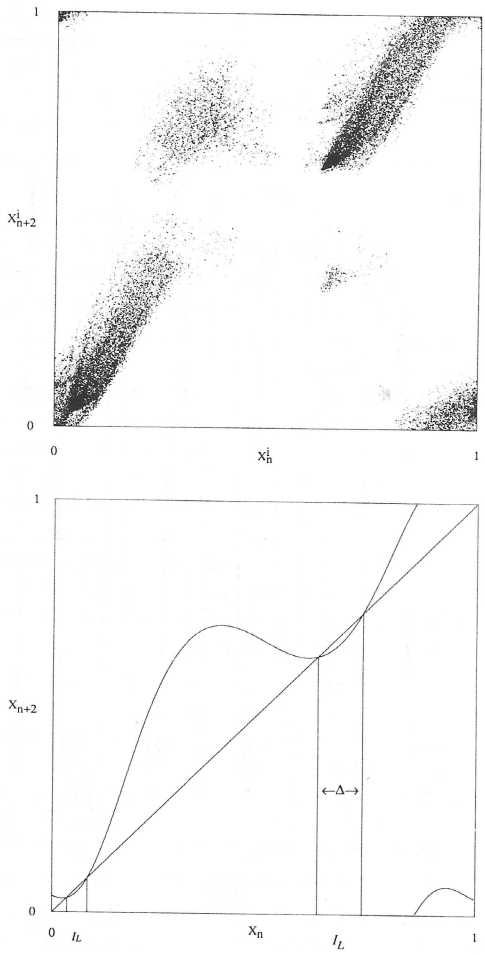

Figure 34. Temporal return map (top) for the lattice of the preceding figure. Two-step temporal return map plotted for N lattice sites over 256 time steps. This then shows the second iterate of the effective local dynamics. The two darkened triangular regions are concentrated at the two fixed points of the isolated circle map. The lower figure shows a plot of the second iterate of the local circle map dynamics at the same parameter values (k = .2 and ω = .55). This illustrates the structure of the two intermittency channels I_L of width Δ.

bursts. The bursts propagate in space-time intermittently. In wavenumber space, the time-averaged spectrum of the burst motion has a peak at k = 0 surrounded by a broad-band component, while the pattern's periodic structure yields a peak at k = K. The phenomenon can be regarded approximately as the competition of two patterns, i.e. one spatially complex at k = 0 and another periodic at k = K. Some examples of this phenomenon are shown in figures 35 and 36 using space-time diagrams. Preliminary investigations of the temporal dependence of the $k \approx K$ mode amplitude indicate that the intermittency is characterized by low temporal frequency noise.[69,70]

At an appropriate coupling strength ε, two spatial modes compete. For example, at ε = .03 the mode with a wavelength of 8 sites and one of 6 sites compete as can be seen in figure 36. At smaller nonlinearity r, these two modes stably exist and form a static pattern. At the parameter used in figure 36, frustration due to the pattern competition causes a burst to develop and propagate, destroying any regular spatial pattern. As the nonlinearity is increased, the pattern loses stability and collapses spontaneously into "fully-developed turbulence". In the latter regime, no peaks are observed in the spatial power spectrum.

The detailed mechanism of this intermittency has not yet been clarified. The phenomena, however, are observed in fairly large regions of parameter space. Additionally, it is readily observed in video feedback studies of the effects of rotational boundary conditions on pattern symmetry. In this two-spatial-dimension system, the dominant spatial wavenumbers are easily controlled by the image rotation.[57]

7. OPEN FLOW LATTICES

In the present section, lattice models with asymmetric coupling are investigated. This class is architecturally related to the multiple time-scale intermittency models[82] briefly mentioned above. When the latter are temporally discretized the hierarchy of driver-drivee relationships produces uni-directional coupling between the local dynamical systems.[1] Here, however, we shall interpret the hierarchy of systems as a single spatially-extended system.

For the class of open flow models considered in this section, the degree of unidirectional coupling is explicitly controlled by an asymmetry parameter α. The model is given by

$$x_{n+1}^{i} = f(x_n^i) + \varepsilon\{\alpha f(x_n^{i+1}) + (1-\alpha) f(x_n^{i-1}) - f(x_n^i)\}$$

In the following we shall study the extreme case $\alpha = 0$, where the coupling is uni-directional, going only from left to right.

One motivation for asymmetric coupling is to understand the behavior of continuum models with first order spatial derivatives in which there is a preferred direction along which perturbations are amplified. A typical example is the open fluid flow system, which is one of the most well-known examples of turbulence. This type of system has not yet been studied in detail from the viewpoint of dynamical system theory.

Here we study mainly the case with $f(x) = rx(1-x)$ and additive future-coupling.[54] Analogous behavior to that described in the following is found in the asymmetric additive (non-future-coupled) logistic lattice.[1] Deissler[85] constructed an open flow model

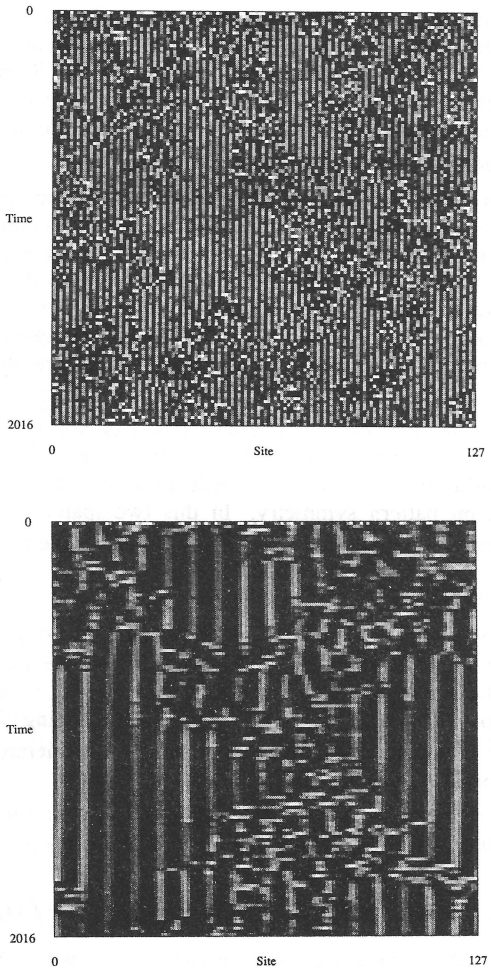

Figure 35. Space-time diagrams of site amplitudes in the range [.1,1.]. The system here is the Laplacian future-coupled logistic lattice with 128 lattice sites starting from a random initial condition. The figure details are as follows. All start from the same random initial condition, plotting every 16^{th} step until time $16 \cdot 126$. $k = 3.93$ and $\varepsilon = .1$ (top); $k = 3.83$ and $\varepsilon = .5$ (bottom).

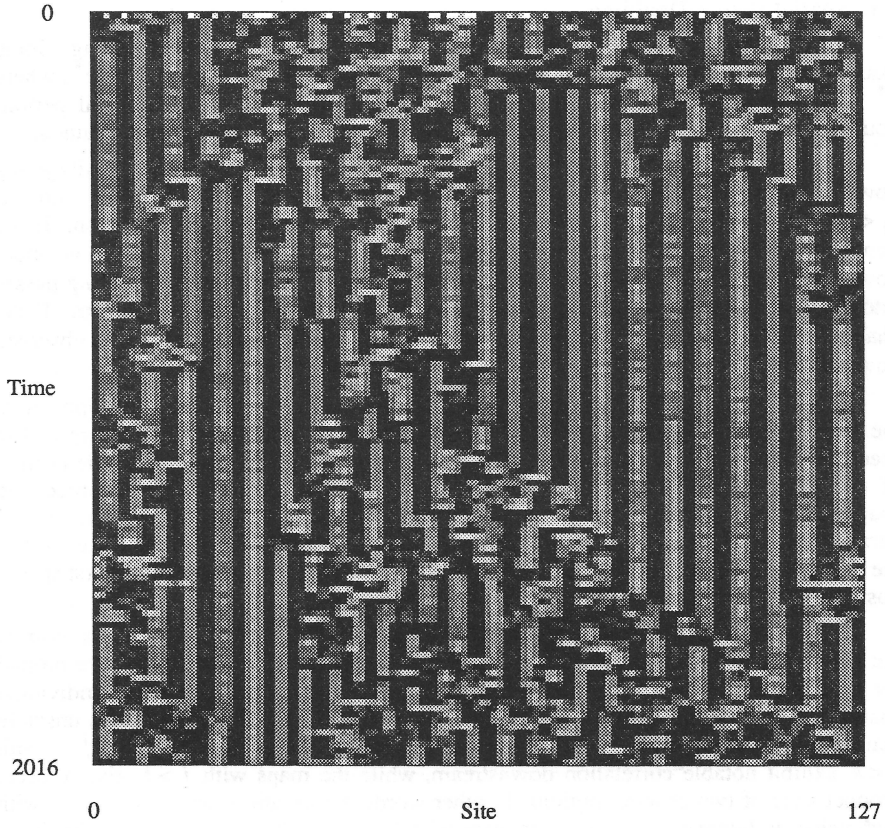

Figure 36. Details as in the preceding figure, except here k = 3.82 and ε = .3.

that is in some sense "dual" to the lattices we describe here: using asymmetric cubic nonlinear coupling and trivial local dynamics. The nonlinear coupling is designed to spatially amplify upstream fluctuations; one artifact of this is the appearance of large and inessential discontinuities in the spatial pattern. The same phenomenology is observed, however, in the simpler asymmetric logistic lattice without the problematic discontinuities.

7.1. Spatial Period-Doubling

One remarkable phenomenon in open flow lattices is spatial period-doubling. Some examples are shown in figures 37 and 38. The left boundary condition is $x^0 = x^*$, where x^* is the unstable fixed point for the logistic map, i.e., $x^* = 1 - r^{-1}$. Spatial period-doubling still occurs if x^0 is different. The right boundary condition is unconstrained.

The spatially period-doubled pattern characteristically develops in complexity going downstream to the right. At lattice sites $0 < i < i_1$, x^i is a fixed point, while at $i_1 < i < i_2$, x^i is a period-two cycle, at $i_2 < i < i_3$ period-four cycle, and so on. If the nonlinearity r is not sufficiently large, x_n^i is period 2^{k+1} for some $i > i_k$ and no more downstream bifurcation occurs. If the nonlinearity r is large, the period-doubling passes into chaos at some order and the pattern is turbulent for $i > i_c$, i.e. downstream. If the chaotic behavior occurs upstream, at $i = i_2$ (say), periodic behavior cannot be observed downstream, $i > i_2$.

The spatial pattern bifurcation diagram of figure 39 illustrates the development of the spatial period-doubling to chaos transition as a function of the nonlinearity r. The preceding amplitude-space plots correspond to parameter setting near the middle portion of the bifurcation diagram. After 256 transient iterations of the 256 site lattice, the spatial pattern is shown in gray scale for site values in the range [.2,1]. The overall parameter-space self-similarity of this transition is evident in the smooth compression of the periodic domains with increasing nonlinearity and in the movement of the first spatial position where chaos is observed.

Figures 40 and 41 present several mosaics of space-time return maps to demonstrate the downstream flow of information. In these, return map points (x_n^i, x_{n+k}^{i+j}) are plotted for j, k = {0, 1, 2, 3} collected over a space-time region. Geometrically, an individual spatial period-doubling pattern lies along a curve that is one of the attractor's unstable manifolds in the full state space. The space-time return maps for x_n^i versus x_{n+k}^{i+j} with $j < k$ exhibit notable correlation downstream, while the maps with $j > k$ give a direct product state of two chaotic motions. In other words, information cannot propagate with high velocity. Interestingly, the return maps with $(j = 0, k > 2)$ are also close to the direct product state, that is, very slow information propagation is also forbidden. This is consistent with the observation that disturbances propagate only within specific velocity bands.[35,86]

7.2. Spatial Amplification of Fluctuations

The patterns in open flow systems are dominated by spatial instability, where a perturbation grows as it moves downstream.[87] In this case, even if a state is stable in the stationary frame, the state can become unstable downstream by amplification of very small fluctuations, including numerical round-off error. This property can be analyzed in

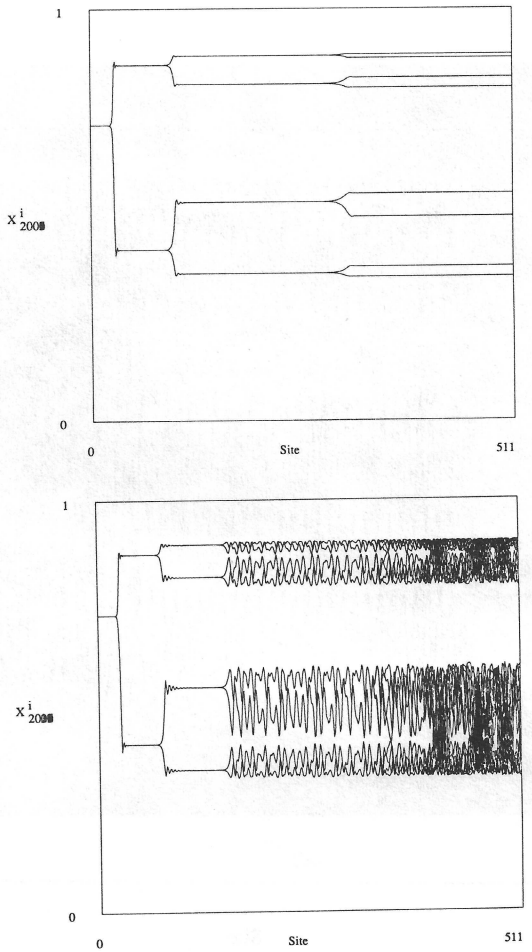

Figure 37. Amplitude-space plots for the unidirectionally future-coupled logistic lattice with 512 sites. The coupling strength was $\varepsilon = .5$. In each plot 32 time steps are overlaid after 2000 transient iterations. The initial condition was random with mean equal to the unstable fixed point x* and with standard deviation .01, where $x^* = 1 - r^{-1}$. The boundary condition at site 0 is $x^0 = x^*$ and at the rightmost site is unconstrained. Individual figure details are as follows. The nonlinearities are r = 3.56 (top) and r = 3.60 (bottom).

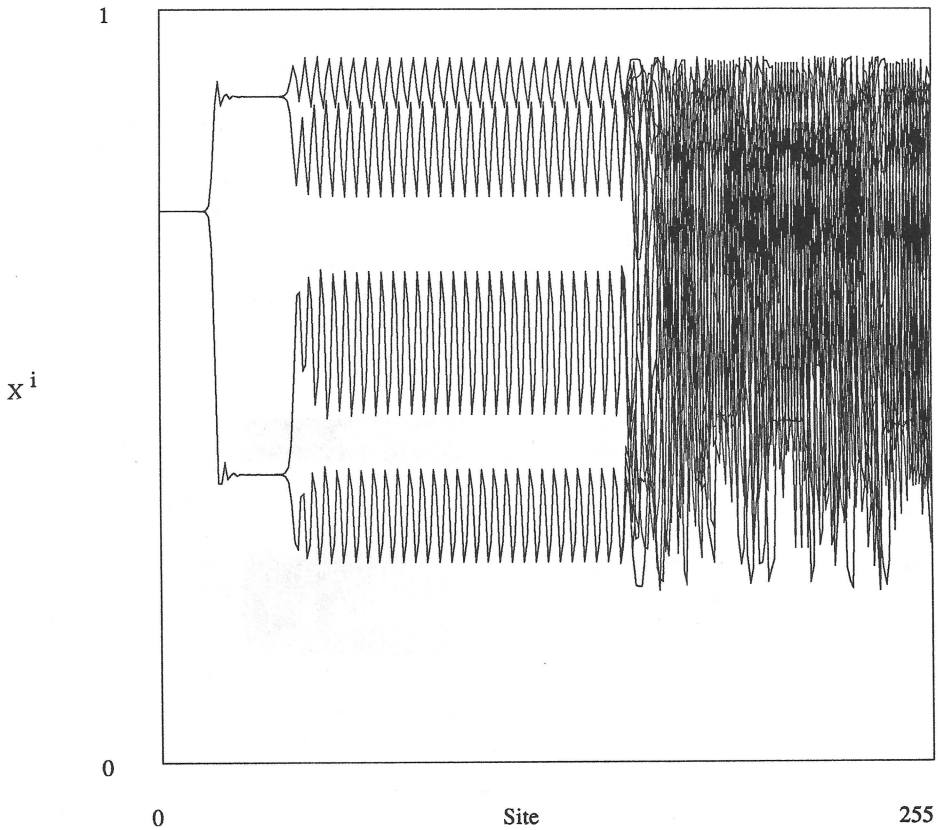

Figure 38. Same details as in the preceding figure, except with higher nonlinearity r = 3.75 and 256 sites.

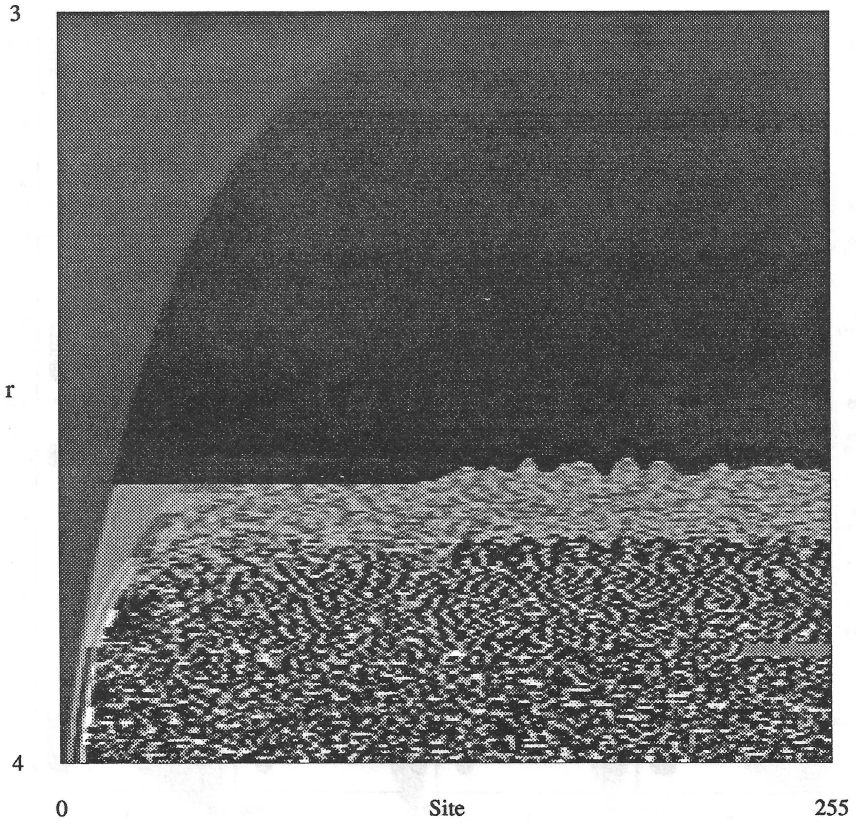

Figure 39. Spatial pattern bifurcation through the period-doubling cascade to chaos in the logistic open flow lattice. The nonlinearity parameter varies from r = 3 to r = 4 in 256 increments. After 256 transient iterations of the 256-site lattice, the spatial pattern is shown in gray scale for site values in the range [.2,1]. The asymmetry parameter $\alpha = 0$, yielding right-only moving perturbations, and the coupling is $\varepsilon = .5$. As before, the left boundary condition is fixed at the logistic map's unstable fixed point, which depends on r. And the right boundary condition is free.

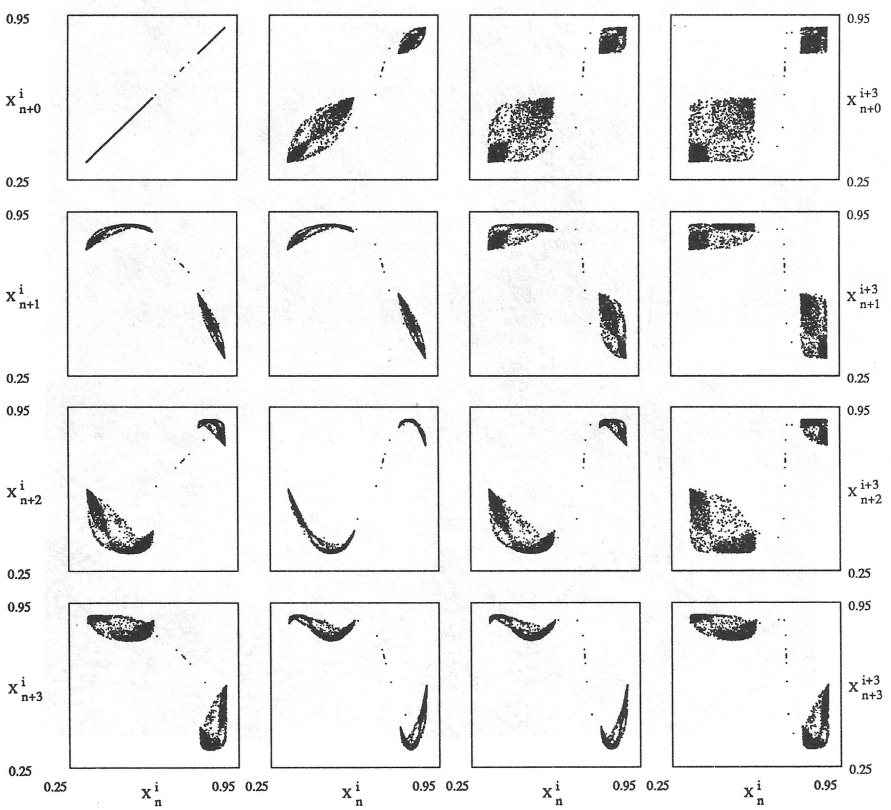

Figure 40. Space-time return map mosaic for the behavior in the preceding figures. 32 time steps are overlaid in each and points are collected from for N-j sites. There are 512 sites, $\varepsilon = .5$, and the nonlinearity $r = 3.6$. The systems were iterated 2000 time steps to allow for the decay of transients. This and the following mosaic show return maps for (x_n^i, x_{n+k}^{i+j}) with j, k $\in$ [0,3].

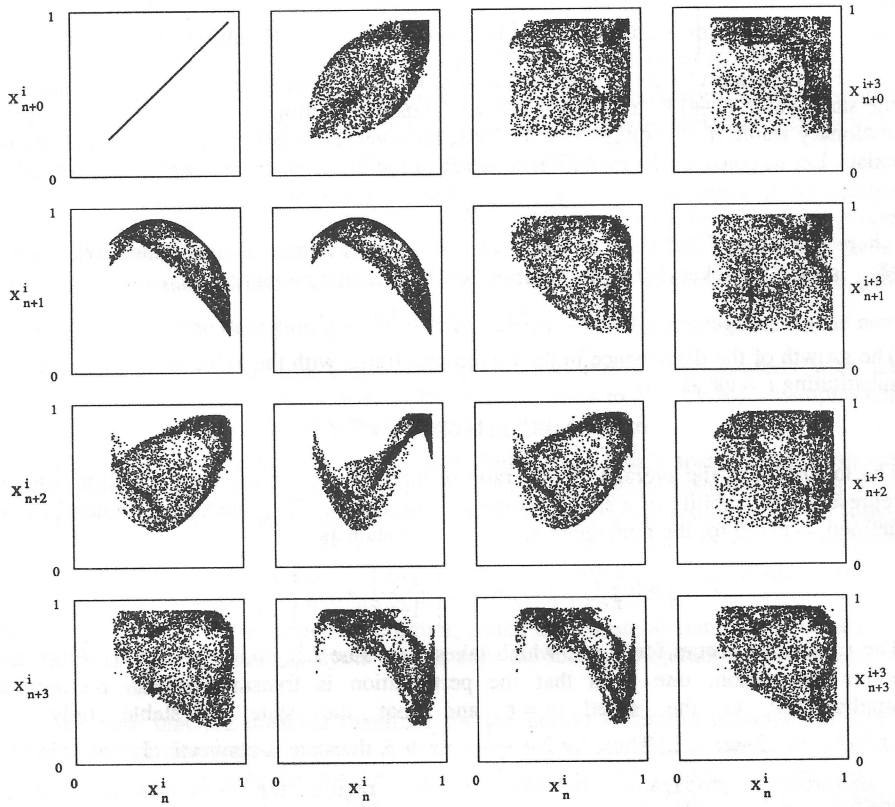

Figure 41. Details as in the preceding figure, except the nonlinearity has been increased to r = 3.75.

a some detail for the uni-directional coupling model in which $\alpha = 0$.

First, we consider the stability of a homogeneous fixed point state, i.e., $x^i = x^*$. The Jacobi matrix for the model is given by

$$J = \begin{bmatrix} (1-\varepsilon)f'(x^1) & \varepsilon f'(x^2) & 0 & \cdots & 0 \\ 0 & (1-\varepsilon)f'(x^2) & \varepsilon f'(x^3) & \cdots & 0 \\ \cdots & \cdots & \cdots & \cdots & \cdots \\ 0 & 0 & 0 & \cdots & (1-\varepsilon)f'(x^N) \end{bmatrix}$$

For the state $x^i = x^*$, the eigenvalues of the matrix are degenerate and they all take the same value $(1-\varepsilon) f'(x^*) = (1-\varepsilon)(2-r)$. Thus, the homogeneous state is stable in the stationary frame if $|(1-\varepsilon)(2-r)| < 1$. This, however, does not mean that the state stably exists. Let us consider the evolution equation of the disturbance δx_n^i, which is given as

$$\delta x_{n+1}^i = A\,\delta x_n^i + B\,\delta x_n^{i-1}$$

where $A = (1-\varepsilon) f'(x^*)$ and $B = \varepsilon f'(x^*)$. If we start from the disturbance $\delta x_0^i = d\,\delta_{i,0}$ ($\delta_{i,j}$ is the Kronecker delta), the solution for the preceding equation is

$$\delta x_n^i = \binom{n}{i} A^{n-i} B^i$$

The growth of the disturbance in the co-moving frame with the velocity v is obtained by substituting $i = vn$ as

$$\delta x_n(vn) = \binom{n}{vn} (1-\varepsilon)^{(1-v)n}\, \varepsilon^{vn}\, f'(x^*)^n \,.$$

The logarithm of the average growth ratio of the perturbation per time step (for large n) represents the stability of a state in some moving frame. The ''stability exponent'', thus defined, is given for the homogeneous fixed point state as

$$L(v) = \log |f'(x^*)| + \log \left| \frac{1-\varepsilon}{1-v} \right| + \log \left| \frac{\varepsilon(1-v)}{v(1-\varepsilon)} \right|^v$$

The maximum occurs for $v = \varepsilon$, which takes the value $L_{\max} = \log |f'(x^*)|$. From the above calculation, one finds that the perturbation is transmitted with the largest amplification at the speed $v = \varepsilon$ and that the state is stable only for $|f'(x^*)| = |2-\alpha| < 1$. Thus, for $2 + \dfrac{1}{1-\varepsilon} > r > 3$, the state is convectively unstable and a perturbation propagates. In this parameter region, the homogeneous state is exponentially unstable and so is susceptible to very weak noise and numerical error. The simulation started from the homogeneous solution $x^i = x^*$ in the parameter regime where the solution is unstable only in the moving frame. Rigorously speaking, the state should remain fixed. In simulations, however, the errors introduced in the last digit ($\sim 15^{th}$, for example, in double precision IEEE format) during the computation makes the state unstable and spatial period-doubling proceeds after only a small number of lattice iterations. The microscopic fluctuations at the fixed boundary are macroscopically manifested via this spatial amplification mechanism. In physical systems, ever-present microscopic fluctuations render convectively unstable states observable.

The stability of a homogeneous periodic state is calculated in a similar manner. The stability exponent in the co-moving frame is given by

$$L(v) = L_0 + \log\left|\frac{1-\varepsilon}{1-v}\right| + \log\left|\frac{\varepsilon(1-v)}{v(1-\varepsilon)}\right|^{v}$$

where L_0 is the stability exponent for the given cycle for the one-dimensional map $x_{n+1} = f(x_n)$ (i.e., $\frac{1}{p}\log|f'(x_1)f'(x_2)\cdots f'(x_p)|$ for the cycle $x_2 = f(x_1), x_p = f(x_{p-1})$, and $x_1 = f(x_p)$). The maximum $L(v)$, L_0, again occurs at $v = \varepsilon$. Thus, the periodic state with period 2 successively attains convective instability at the same parameter that the period-doubling bifurcation occurs in the logistic map $x_{n+1} = f(x_n)$. For the homogeneous chaotic state the same formula for $L(v)$ applies.

The above calculation is valid only for a locally homogeneous state. If spatial inhomogeneity appears, the analytic calculation is difficult at best, and one must resort to numerical calculation of the co-moving Lyapunov exponent.[35,86]

The mechanism for spatial period-doubling is understood in terms of convective instability as follows. Assume that the state at x_n^i is very close to the cycle with period 2^k. If the cycle is convectively unstable with the stability exponent $L_{\max} = L(v^*)$, the deviation is enhanced with the factor $e^{L_{\max}}$ for one iteration as it goes downstream with the speed $v^* = \varepsilon$. The deviation thereby is enhanced by $\frac{e^{L_{\max}}}{v^*}$ for propagation to the next lattice site and the next time step. The spatial period-doubling proceeds with the successive convective instability of each 2^k-cycle: 2^k leads to 2^{k+1} cycles. It stops when the cycle is stable, that is when the associated $L_{\max} < 0$.

The instability of a periodic state is amplified along a kink's spatial locus as shown in figure 42. There, transients are shown with spatial return maps during time steps 50 to 100 and 150 to 300, respectively. After the transients have died out the spatial return map gives the pattern in figure 43. In figure 42 (bottom) we can see the unstable manifold from period-1 domain, which comes into the period-2 domain along the latter's stable manifold. The period-2 domain in turn exhibits the amplification of instability as is seen in the curve at the left side of the figure, which is its unstable manifold. The process continues to up to a period 2^k cycle, that is until the local configuration is stabilized, or until it becomes chaotic.

We note that the unstable manifold for the period-1 domain coincides with the stable manifold for period-2, which is *transverse* to the unstable manifold of period-2 domain. This point is essential for the process of spatial period-doubling in open flow. It suggests a geometric picture of perturbation flow along a hierarchy of local unstable submanifold connections in the high-dimensional state space.

The size of each cycle's domain is roughly estimated from the above argument. The scaling relation above, however, seems to be difficult to observe, since the effect of small noise dominates in the convectively unstable case. For example, the lattice point at which the period-doubling occurs varies with the simulation's precision and the round-off algorithm. Thus, just as in following a particular trajectory in a low-dimensional chaotic system, different machines produce different patterns. As in preceding studies of chaos, however, the ultimate goal is not to suppress this property, but to study its qualitative scaling features over a range of precision and external noise levels.

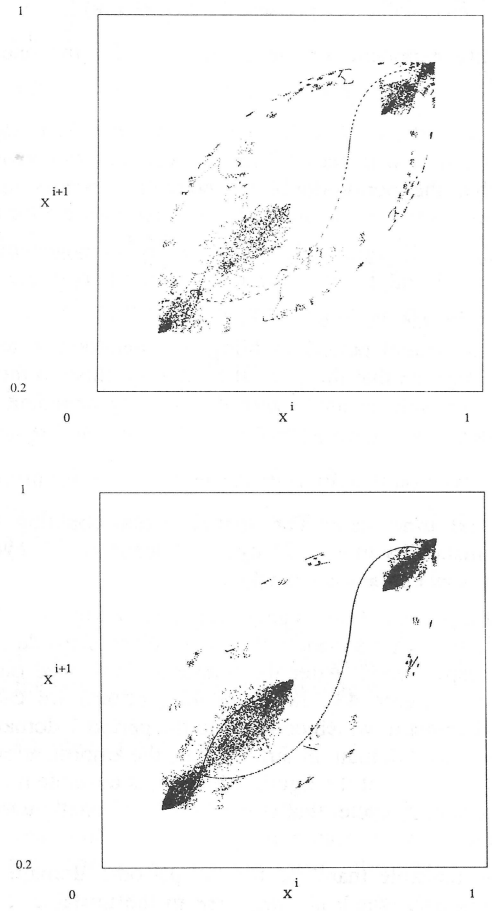

Figure 42. Spatial return maps for the uni-directionally additive future-coupled logistic lattice with r = 3.6, ε = .5, and N = 128 sites. Initial and boundary conditions are same as in preceding figures. The return map points (x^i, x^{i+1}) are collected from N-1 sites. The durations for each figure are from step 50 to 100 (top) and from 150 to 300 (bottom).

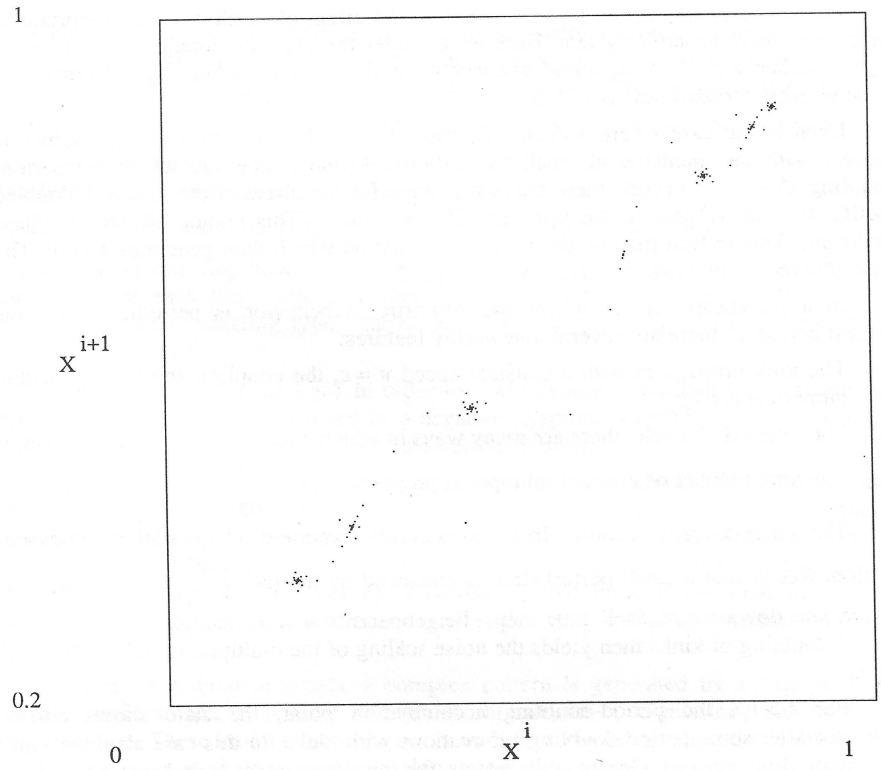

Figure 43. Details as in the preceding figure, except here the points are shown during steps from 1500 to 1530. Here, all the transients have died out, leaving points on the attractor itself.

This spatial unpredictability in open flow lattices has an origin similar to that in low-dimensional chaos, but it is manifested graphically in real space. More importantly, this phenomenon provides a clear demonstration of the additional mechanism operating in spatially-extended nonlinear systems: the spatial transmission of information. This mechanism is responsible for the appearance of complex patterns.

7.3. Domain Walls and Kink Dynamics

As was discussed in the previous section, the effect of small noise is important in the convectively unstable system. Here we consider the uni-directionally future coupled logistic lattice with noise σ_n^i added at every site and every step, where σ_n^i is δ-correlated noise uniformly distributed in $(-\sigma,\sigma)$.

Even in the case where a cycle of period 2^k is stable, a remarkable phenomenon appears with the inclusion of small fluctuations. At the lattice site where the period-doubling $2^k \to 2^{k+1}$ occurs, there are two choices for the phase of the resulting doubled oscillation with respect to the upstream 2^k oscillation. This choice allows for phase switching. This in turn may be driven by a fluctuation which then generates a kink. The kink then moves downstream with constant speed.

In a parameter regime where the downstream behavior is periodic with some longest period 2^k there are several noteworthy features:

(i) The kink propagates with a constant speed $v = \varepsilon$, the coupling strength (to within numerical error);

(ii) For a period 2^k cycle, there are many ways in which a kink can change phase; and

(iii) The total number of kinks of all types is proportional to $\dfrac{1}{\log\sigma^{-1}}$.

The latter estimate follows from the stability exponent analysis of the previous section. Recall that a small perturbation is enhanced by the factor $\dfrac{e^{L_{\max}}}{v^*}$ in moving one lattice site downstream each time step. Feigenbaum's scaling analysis applied to the period-doubling of kinks then yields the noise scaling of the multiplicity of possible kink types.

For $r > r_c$, the period-doubling accumulation point, the state shows chaotic behavior after some period-doubling bifurcations with kinks. In this case also, the kinks propagate downstream. One notable feature for the downstream turbulence beyond the spatial period-doubling is its further insensitivity to the external noise level.

A pattern's downstream flow is revealed in a co-moving reconstruction of the dynamics.[35] If the co-moving velocity is slower or faster than the maximum perturbation propagation speed, the reconstruction is essentially the direct product of two independent dynamics. The reconstruction corresponding to the maximum perturbation velocity $v \simeq \varepsilon$, in contrast, indicates strong correlation. (Recall the space-time return map mosaics of figures 40 and 41.) Information propagation using mutual information has been studied by the authors, see reference (35) as an example. A more thorough investigation is presented elsewhere.[32]

8. TRANSIENT SPATIAL CHAOS

As a simple example of spatio-temporal complexity arising in a nonlinear lattice that is *not* associated with an attractor, we study in this section a model exhibiting *transient spatial chaos*. The lattice is the piecewise-linear ''dripping handrail'' model,[88] which is given by a future-coupled lattice with the local dynamic

$$f(x) = sx + \omega \ (mod\ 1)$$

This local dynamic is essentially a circle map with zero nonlinearity parameter k and with additional control of the slope s. The local dynamics consists of the constant increase by ω with each iteration and a sudden decrease in amplitude above a ''threshold'', $x_{threshold} = \frac{1-\omega}{s}$. The first process models the increase of the hanging water layer's thickness, assuming there is a constant rate of flow onto the handrail. While the second process, (mod 1), corresponds to the decrease in local water mass by drops breaking away and falling. A future-coupled totalistic kernel, $\vec{\varepsilon} = (-\frac{2}{3}, \frac{1}{3}, \frac{1}{3})$, mimics the replenishing flow of water along the handrail by a simple low pass filtering of the pattern at each time step. The analogy of this model with the dripping handrail phenomenon and ''sizzling type'' turbulence was originally suggested by Rössler and one of the authors.[88]

Here we treat the case $s \leq 1$ in order to study dynamics without local information production. The latter is guaranteed by a negative Lyapunov spectrum. We note also that the isolated local dynamic exhibits a stable period 25 orbit.

Typical evolution from a random initial condition is shown with a space-time diagram in figure 44. Detailed investigation of this model indicates that the apparent complexity is due only to a nonlinear superposition of patterns that emanate from the initial condition. This is highly reminiscent of class-3 cellular automata. One important similarity of this model and cellular automata is that there is no local information production and that the apparent complexity is due only to the information mixing in space.

In class 3 cellular automata, a complex pattern is generated by a ''single seed'' initial condition via a process of spatial information transmission and nonlinear superposition. These initial conditions are characterized by being algorithmically simple. The evolution, nonetheless, produces algorithmically complex patterns. In the present model, also, a single seed initial condition gives rise to the propagation of complex patterns (see figure 45), where the initial condition is $x^{63} = .4$ and $x^{i \neq 63} = .3$ in a lattice of 128 sites.

The spatial and temporal return maps are given in figure 46. We note the ''whiskers'' stemming from the line with $x^i = x^{i+1}$, which correspond to localized dripping.

When the slope is less than unity, the state is ultimately attracted into a periodic cycle. The attractor's period and the transient length increase with lattice size apparently exponentially. In cellular automata, also, the state is ultimately attracted into a cycle if the system has finite size. A similar dependence of transient length on system size is found in some classes of cellular automata.[89] To illustrate the growth of transient time for

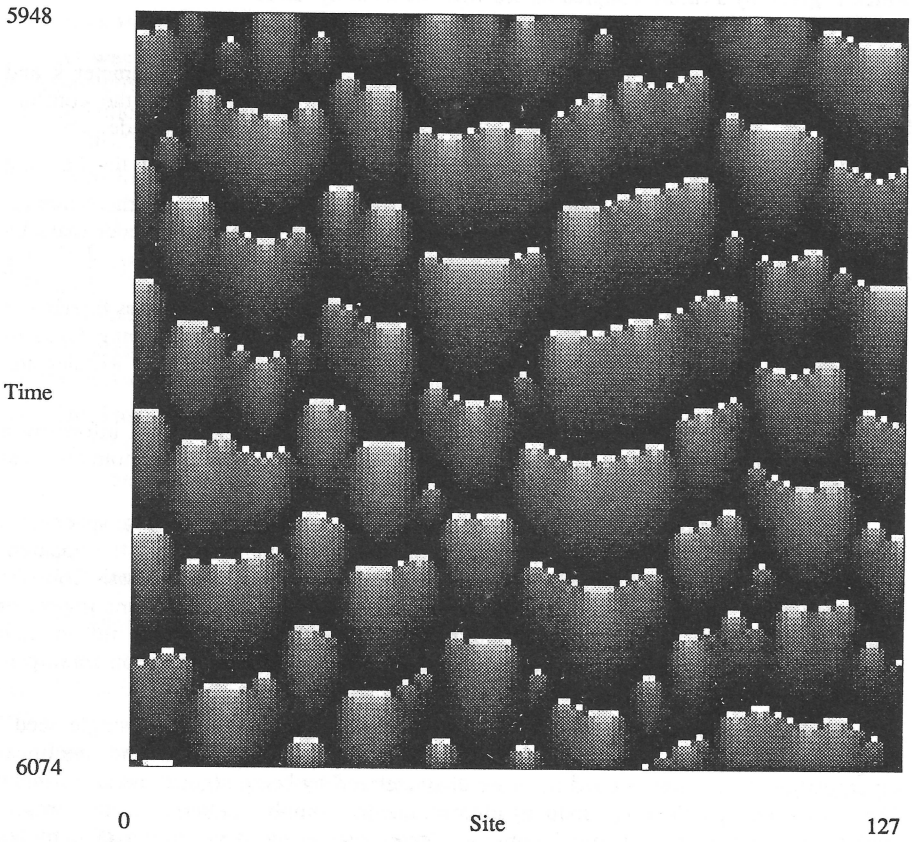

Figure 44. Space-time diagram with site amplitudes plotted in the range [0,1] for the dripping handrail model with s = .91, ω = .1 and 128 lattice sites. A uniformly distributed random initial condition with mean .3 and standard deviation .1 was used. 128 steps are shown, after approximately 6000 transient iterations.

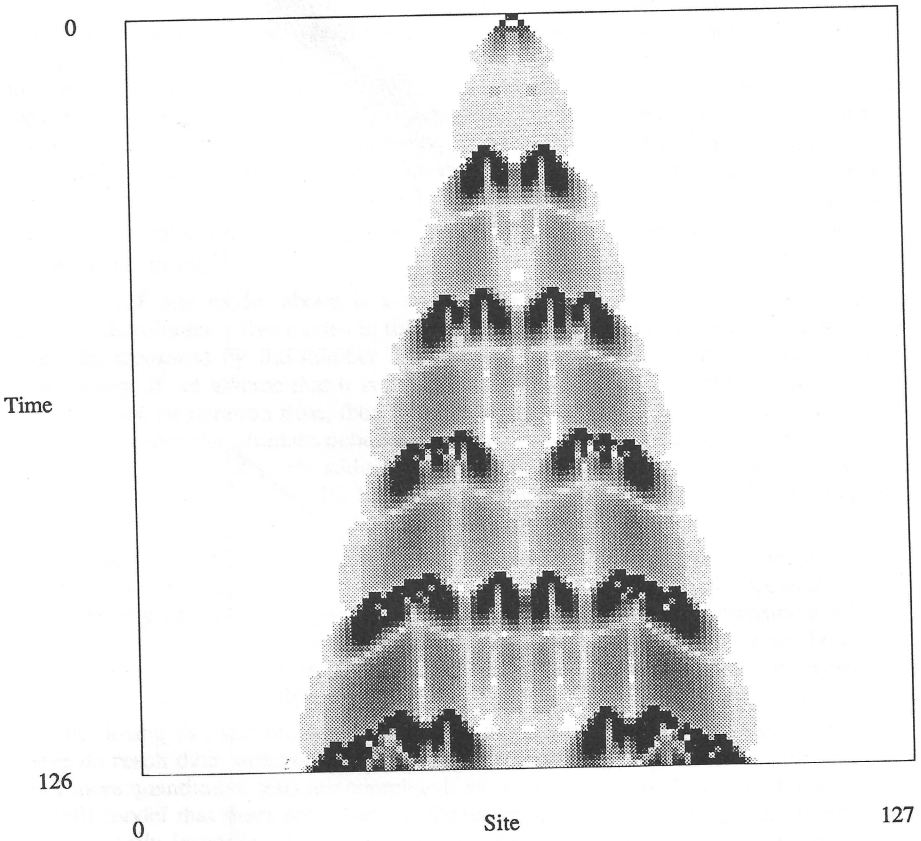

Figure 45. Space-time diagram with the absolute value of spatial differences plotted in the range [0,.1] for the same model with same parameters as in preceding figure. The algorithmically-simple initial condition consists of sites at $x^{i\neq 63} = .3$ except for the middle lattice site 63, where it takes the value $x^{63} = .4$. The diagram shows the development and propagation of spatial perturbations from the initial pattern.

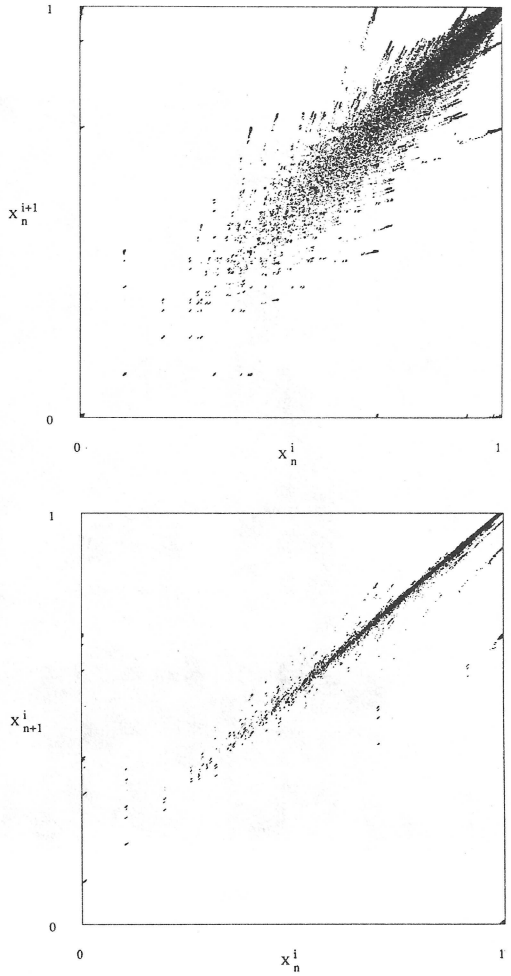

Figure 46. Return maps for the dripping handrail. (top) The spatial return map for N-1 sites collected during 32 time steps. (bottom) The temporal return map for 128 time steps collected over the entire lattice.

this lattice example, space-time diagrams are shown for N = 8, 16, and 24 in figures 47 and 48, during transient decay and after they have died away. The increase of transient length and attractor period is clearly seen.

This example of apparently complex, but transient, spatial chaos is a disturbing comment on the recent endeavor to view fluid turbulence, to take a notorious example, in terms of (chaotic) attractors. This example demonstrates that complex behavior in a spatial system may be dominated by very long transients; transients potentially so long that the system state may never reach the attractor. In this case, the attractor's properties may have nothing what-so-ever to do with any observable behavior. If so, it is a moot point, indeed, whether or not the attractor is chaotic. The asymptotic invariant measure supposedly governing fluid turbulence may never be reached in practical time. This kind of long-lived complex transient pattern evolution can be seen also in the previous examples of pattern competition, in some partial differential equations,[90] and in video feedback dynamics.[23]

The 128 site model above is a small system in comparison with the number of spatially-distributed active modes in fully-developed turbulent fluid flow. (The latter size might be measured by the number of dissipation-scale eddies contained in the flow.) Nonetheless, if we assume that it is a physical model with a characteristic time of (say) 10^{-9} seconds, its iteration time, then an experimenter would still have to wait a year and a half to observe the ultimate periodic attractor, even in a mathematically ideal setting. (We assume in this that every addition of 8 sites to the system size increases the average transient length by a factor of 10. Exponential growths rates larger than this are indicated by our finite-size scaling studies.)

Aside from a better quantitative characterization of this phenomenon, we need to determine when such behavior might occur. Most likely this will demand a better understanding of basin structure organization in these very-high dimensional systems. This, then, will have to be interpreted in light of estimates of the upper bounds on attractor dimensions, that is, the number of active modes, to fully appreciate the implications for fluid turbulence.

In closing this section, we should recall that many of the spatial systems described above *do* reach their attractor in finite time, i.e. thousands of iterations usually, not 10^{16}. Until more quantitative tests are completed, we wish only to emphasize with the dripping handrail model that there are other significant effects appearing in spatial systems than those typically investigated in low-dimensional dynamical systems. The study of these prototype models will be very helpful in unraveling some of these new and difficult problems.

9. SUMMARY

With this brief survey, we have covered a variety of phenomena in spatio-temporal chaos that arises in the class of discrete time and space lattice dynamical systems. These included the period-doubling and merging of domains and kinks, spatial-mode instability and spatio-temporal quasi-periodicity, soliton turbulence, spatial and spatio-temporal intermittency, spatial period-doubling in open flows, and the generation of transient complexity by spatial information transmission. Though we have illustrated these phenomena mainly with the use of coupled logistic and coupled circle lattices, these

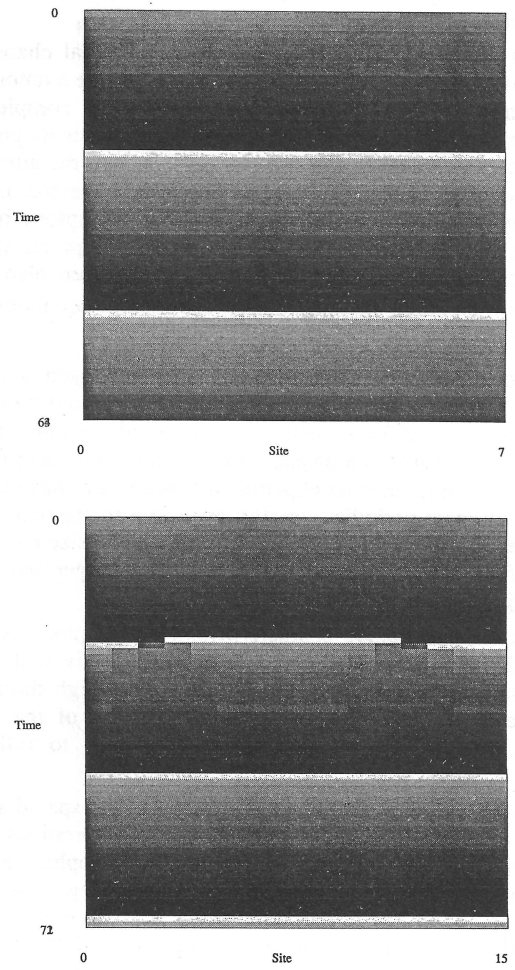

Figure 47. Space-time diagrams with site amplitudes plotted in the range [0,1] for the dripping handrail model. Starting from statistically similar initial conditions, the set of figures illustrates the increasing length of transients with increasing lattice size. The particular details of each figure are as follows. Above there are 8 lattices (top); the diagram shows the first 64 time steps. And, at the bottom the lattice consists of 16 sites; the diagram shows the first 72 steps.

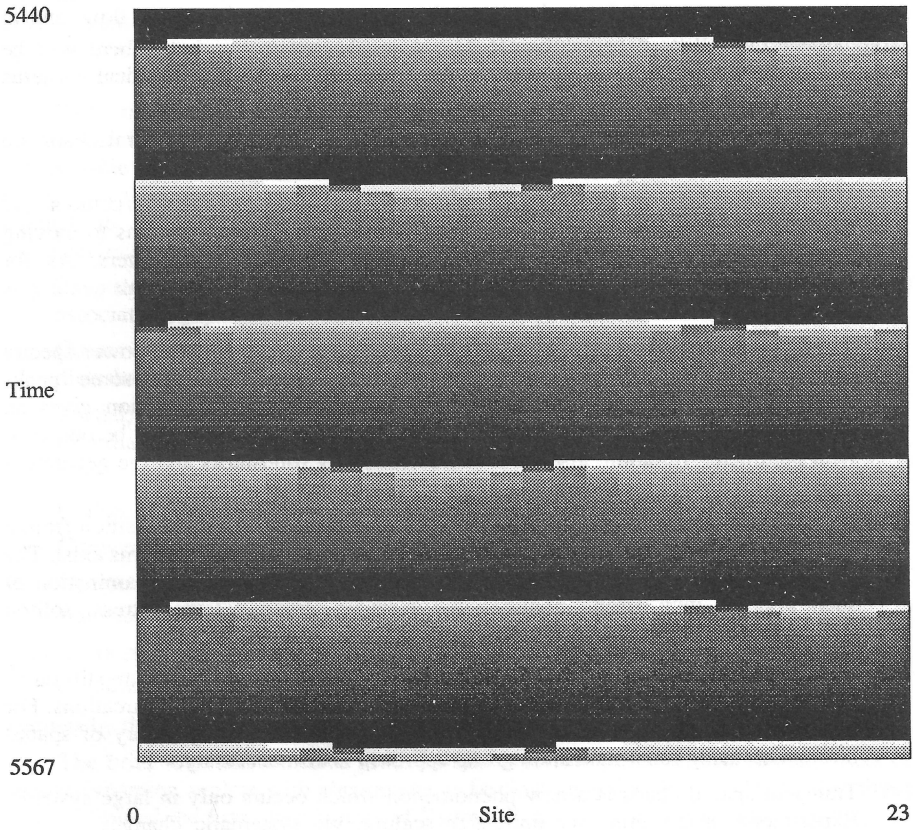

Figure 48. Details as in the preceding figure, except here the periodic behavior during 128 iterations for a lattice with 24 sites is shown after 5440 transient iterations. In each, the ultimate attracting cycle is shown over sufficient time so that one may deduce its period. Note the large jump in transient length required in the last example to reach the attracting cycle.

models appear to be behavioral archetypes for spatio-temporal chaos, generally. We have investigated, in fact, a much wider range of local dynamics and coupling forms and chosen for this essay the simplest models that illustrate widely occurring behavior. Any possible universality is bolstered, as we have occasionally noted, by the experimental observation of several of these phenomena in hybrid electronic-optical video feedback experiments in two spatial dimensions, in large aspect ratio liquid crystal flow, and in large aspect ratio Bénard convection.[91] The new phenomena presented here will be observed, presumably, in the diverse range of spatially-extended physical systems considered in the introduction.

In connection with the experimental observation of the spatio-temporal chaos we have described, a few specific comments are in order.

(i) In the case of period-doubling the direct observation of domain structures and spatial bifurcation will be necessary. The transition from static patterns to moving domains may be observed with the variation of control parameters. As for quantitative comparison, a renormalization group description of kink scaling is necessary.

(ii) In the case of spatial mode instability and intermittency, the spatial power spectra can be obtained using standard methods. The appearance of some peaks accompanied by temporal quasiperiodicity or by phase defect motion gives an example of our spatial mode instability. The pattern competition may be observed with parameter variation, also. It is characterized by robustness and the generation of flicker-like noise for the motion of the corresponding spatial mode.

(iii) Soliton turbulence is typically seen in parameter regimes near the transition from a homogeneous state to fully-developed turbulence, if moving kink patterns exist. The kink patterns are frequently observed in experiments. By detailed examination of such systems with strong nonlinearity or under strong external stress, soliton turbulence will be observed.

(iv) Experiments on open flow systems in the spirit of nonlinear dynamics are still rare.[5] Multipoint probes will be essential to show the existence of spatial bifurcations. For quantitative comparison with theory and experiments, a scaling theory of spatial bifurcation using renormalization group approach is also necessary.

(v) Transient spatial chaos is a new phenomenon which occurs only in large systems. Experiments that mimic our finite-size scaling, via systematic changes in (say) aspect ratio, appear to be the main avenue for observation of the rapid growth in transient durations. Generally speaking, the existence of very long-lived transients should be kept in mind in any experiments on spatially-extended systems for which the goal is to study complex spatio-temporal behavior.

Presenting a much more detailed phenomenology in this didactic form is of somewhat dubious value. Much of the reported behavior can be quickly and interactively explored using personal computers and scientific workstations. This paper should be taken as a guide to this new form of investigation. Even small computers have more than adequate processing power for research on many lattice systems. Indeed, one of the motivations for the invention of this class of dynamical systems was to bring the investigation of many degree of freedom systems to readily available and interactive microcomputers. To date, supercomputers have dominated this research domain. They

do not provide, however, the interactive response and high-graphics-bandwidth demanded by qualitative studies of nonlinear dynamics. Today's small computers do provide the latter and so can support rather large simulation environments, such as *lds,* the one we used. Such an environment allows for ready access to the results presented here and many more detailed and subtle phenomena, without the months of code development typically required for specific numerical projects. Even within a single such environment, if our experience is any indication, there are still many phenomena to be discovered.

From the theoretical side, an encyclopedic accounting of these spatio-temporal phenomena is also not enough. We have tried to point out some directions for analysis and possible limitations. Certainly, further analysis based on the geometric perspective of dynamical systems theory and on an information theoretic approach is a necessary adjunct to a more complete investigation. In the near term the quantitative characterization of spatio-temporal chaos includes the following topics:

(i) Lyapunov spectra for spatially-extended systems, their morphology and that of the associated Lyapunov vectors;

(ii) Co-moving Lyapunov exponents and the propagation speed and direction of disturbances;

(iii) Spatial, spatio-temporal entropies and dimensions and their densities and spatial information flow using multipoint-probe mutual information statistics; information flux;

(iv) Connection with the thermodynamic formalism;[92]

(v) Conventional space-time power spectral analysis;

(vi) Coarse graining and scaling and renormalization group analysis based on the statistical mechanics of spin systems;[93] and

(vii) Reconstruction of spatial dynamics and the deduction of the spatio-temporal equations of motion.[36]

Sequels by the authors pursue these directions.[32,34]

The brief tour that we have given in this overview points to even larger vistas of spatial dynamics, replete with phenomena as fascinating and as little understood as those that confronted the first investigators of "simple", temporal chaos. In our own ongoing studies, we have barely begun to touch on the effects of two and higher spatial dimensions or of other interconnection architectures on the types of instabilities. The former promises new topological structures more complex than the kinks and "solitons" seen in one-dimension. The latter suggests new approaches to the complex problems of life itself using *morphogenetic dynamical systems* to investigate developmental, evolutionary, and learning processes.

ACKNOWLEDGMENTS

The authors thank Rob Shaw and Norman Packard for useful discussions and critical comments. They also thank Carson Jeffries, Harry Lam, and Jeff Tennyson, for comments on the draft manuscript. JPC would like to thank Carson Jeffries for

stimulating discussions and his continuing support. KK is also grateful to Shinji Takesue, Kensuke Ikeda, Masaki Sano, and Yoji Aizawa for critical comments and to Robert Deissler, Doyne Farmer, and Gottfried Meyer-Kress for useful discussions.

JPC's work was partially supported by the Office of Naval Research (N00014-86-K-0154) and postdoctoral fellowships from International Business Machines, Corporation, and the Miller Institute for Basic Research in Science. KK's work was partially funded by the cooperative research program at Institute of Plasma Physics at Nagoya, by the ISM cooperative research program, and by the scientific research fund of the Ministry of Education, Science, and Culture. Last but not least, KK is thankful to Carson Jeffries and his group at UC Berkeley for their kind hospitality during his stay at the University of California, Berkeley.

REFERENCES

1. J. P. Crutchfield, **Noisy Chaos,** Ph.D. Dissertation, University of California, Santa Cruz (1983).

2. K. Kaneko, **Collapse of Tori and Genesis of Chaos in Nonlinear Nonequilibrium Systems,** Ph.D. Dissertation, University of Tokyo, Tokyo (1983).

3. E.N. Lorenz, "Deterministic Nonperiodic Flow", J. Atmos. Sci. *20* (1963) 130.

4. D. Ruelle and F. Takens, "On the Nature of Turbulence", Comm. Math. Phys. *20* (1974) 167.

5. K. R. Sreenivasan, "Transition and turbulence in fluid flows and low-dimensional chaos" in **Frontiers in Fluid Mechanics**, edited by J. L. Lumley, Springer-Verlag, Berlin (1985).

6. V. Steinberg, G. Ahlers, and D. S. Cannell, "Pattern Formation and Wave-Number Selection by Rayleigh-Benard Convection in a Cylindrical Container", Physica Scripta *T9* (1985) 97.

7. D. Ruelle, "Five Turbulent Problems", Physica *7D* (1983) 40.

8. J. R. Pasta, S. M. Ulam, and E. Fermi, "Studies on Nonlinear Problems" in **Collected Works of Enrico Fermi, Vol 2.**, University of Chicago Press, Chicago (1965) 978.

9. N. J. Zabusky and M. D. Kruskal, "Interaction of "Solitons" in a Collisionless Plasma and the Recurrence of Initial States", Phys. Rev. Lett. *15* (1965) 240.

10. C. D. Jeffries and G. Gibson, "Observation of Period Doubling and Chaos in Spin Wave Instabilities in Yttrium Iron Garnet", Phys. Rev. A *29* (1984) 811.

11. C. D. Jeffries, P. Bryant, and K. Nakamura, "Spin-Wave Turbulence", Nuclear Physics *B* (1987) to appear.

12. A. H. Bobeck, "Properties and Device Applications of Magnetic Domains in Orthoferrites", Bell. Sys. Tech. J. *46* (1967) 1901.

13. F. A. De Jonge and W. F. Druyvesteyn, "Bubble Lattices", Proceedings of the AIP 17th Annual Conference on Magnetism and Magnetic Materials (1971) 130.

14. A. Zettl, "Electronic and Elastic Mode Locking in Charge Density Wave Conductors", Physica *23D* (1986) 155.

15. R. Hirota and K. Suzuki, "Studies on Lattice Solitons by Using Electrical Networks", J. Phys. Soc. Japan *28* (1970) 1366.

16. L. A. Ostrovskii, V. V. Papko, and Yu. A. Stepanyants, "Solitons and Nonlinear Resonance in Two-Dimensional Lattices", Sov. Phys. JETP *51* (1980) 417.

17. R. Van Buskirk and C. D. Jeffries, "Observation of Chaotic Dynamics of Coupled Nonlinear Oscillators", Phys. Rev. A *31* (1985) 3332.

18. C. D. Jeffries and G. Held, "Spatial and Temporal Structure of Chaotic Instabilities in an Electron-Hole Plasma in Ge", Phys. Rev. Lett. *55* (1985) 887.

19. R. Rosensweig, **Ferrohydrodynamics,** Cambridge University Press, Cambridge (1986).

20. J. P. Crutchfield and H. Lam, "Ferrohydrodynamic Interfacial Instabilities: Experimental Observations", preprint (1987).

21. D. W. Thompson, **On Growth and Form,** Cambridge University Press, Cambridge (1961).

22. N. H. Packard, "Lattice Models for Solidification and Aggregation", Proceedings of the First International Symposium on Form, Tsukuba, Japan (1985).

23. J. P. Crutchfield, "Space-Time Dynamics in Video Feedback", Physica *10D* (1984) 229.

24. C. Vidal and A. Pacault, eds., **Nonequilibrium Dynamics in Chemical Systems,** Springer-Verlag, Berlin (1984).

25. A. T. Winfree, **The Geometry of Biological Time,** Springer-Verlag, Berlin (1980).

26. A. M. Turing, "The Chemical Basis of Morphogenesis", Trans. Roy. Soc., Series B *237* (1952) 5.

27. T. Kohonen, **Self-organization and Associative Memory,** Springer-Verlag, Berlin (1984).

28. D. E. Rumelhardt and J. L. McClelland, **Parallel Distributed Processing,** MIT Press, Cambridge (1986).

29. J. J. Hopfield, "Neural Networks and Physical Systems with Emergent Collective Behavior", Proc. Natl. Acad. Sci. *79* (1982) 2554.

30. G. B. Ermentrout and J. D. Cowan, "Large Scale Spatially Organized Activity in Neural Nets", SIAM J. Appl. Math. *38* (1980) 1.

31. R. A. Roberts and C. T. Mullis, **Digital Signal Processing,** Addison-Wesley, Reading, Massachusetts (1987).

32. J. P. Crutchfield and K. Kaneko, "Space-Time Information Theory", in preparation (1987).

33. N. H. Packard, J. P. Crutchfield, J. D. Farmer, and R. S. Shaw, "Geometry from a Time Series", Phys. Rev. Let. *45* (1980) 712.

34. J. P. Crutchfield and K. Kaneko, "Statistical and Deterministic Mechanics of Spatio-Temporal Chaos", in preparation (1987).

35. K. Kaneko, "Lyapunov Analysis and Information Flow in Coupled Map Lattices", Physica *23D* (1986) 436.

36. J. P. Crutchfield and B. McNamara, "Equations of Motion from a Data Series", preprint (1986).

37. K. L. Chow and A. L. Leiman, "The Structural and Functional Organization of the Neocortex", Neurosciences Res. Prog. Bull. *8* (1969) 153.

38. J. C. Eccles, M. Ito, and J. Szentagothai, **The Cerebellum as a Neuronal Machine,** Springer-Verlag, New York (1967).

39. W. D. Hillis, "The Connection Machine: A Computer Architecture Based on Cellular Automata", Physica *10D* (1984) 213.

40. W. D. Hillis, in **The Connection Machine**, MIT Press, Cambridge (1986).

41. J. D. Farmer, T. Toffoli, and S. Wolfram, **Cellular Automata, Proceedings of an Interdisciplinary Workshop,** North-Holland Publishing Company, Amsterdam (1984).

42. J. P. Crutchfield and N. H. Packard, "From Cellular Automata to Lattice Dynamical Systems", unpublished notes (1984).

43. P. Grassberger, "Chaos and Diffusion in Deterministic Cellular Automata", Physica *10D* (1984) 52.

44. J. P. Crutchfield, J. D. Farmer, N. H. Packard, R. S. Shaw, G. Jones, and R. Donnelly, "Power Spectral Analysis of a Dynamical System", Phys. Lett. *76A* (1980) 1.

45. B. A. Huberman and J. P. Crutchfield, "Chaotic States of Anharmonic Systems in

Periodic Fields'', Phys. Rev. Lett. *43* (1979) 1743.

46. B. A. Huberman, J. P. Crutchfield, and N. H. Packard, ''Noise Phenomena in Josephson Junctions'', Appl. Phys. Lett. *37* (1980) 750.

47. O. E. Rossler, ''An Equation for Continuous Chaos'', Phys. Lett. *57A* (1976) 397.

48. Y. Kuramoto, ''Instability and Turbulence of Wavefronts in Reaction-Diffusion Systems'', Prog. Theo. Phys. *63* (1980) 1885.

49. A. R. Bishop, G. Gruner, and B. Nicolaenko, **Spatio-Temporal Coherence and Chaos in Physical Systems, Physica 23D,** North-Holland, Amsterdam (1986).

50. H.T. Moon, P. Huerre, and L.G. Redekopp, ''Transitions to Chaos in the Ginzburg-Landau Equation'', Physica *7D* (1983) 135.

51. A.R. Bishop, K. Fesser, and P.S. Lomdahl, ''Influence of Solitons in the Initial State on Chaos in the Driven Damped Sine-Gordon System'', Physica *7D* (1983) 259.

52. J. D. Keeler, ''An Explicit Relation between Coupled-Maps, Cellular Automata, and Reaction-Diffusion Equations'', UCSD preprint (1986).

53. K. Kaneko, ''Period-doubling of kink-antikink patterns, quasiperiodicity in antiferro-like structures and spatial intermittency in coupled logistic lattice'', Prog. Theo. Phys. *72* (1984) 480.

54. K. Kaneko, ''Spatial Period-doubling in Open Flow'', Phys. Lett. *111A* (1985) 321.

55. K. Kaneko, ''Kinks and turbulence in coupled map lattices'' in **Dynamical Problems in Soliton Systems**, edited by S. Takeno, Springer-Verlag, Berlin (1985).

56. J. P. Crutchfield, J. D. Farmer, and B. A. Huberman, ''Fluctuations and Simple Chaotic Dynamics'', Phys. Rep. *92* (1982) 45.

57. J. P. Crutchfield, **Space-Time Dynamics in Video Feedback and Chaotic Attractors of Driven Oscillators,** video tape, Aerial Press, P.O. Box 1360, Santa Cruz, CA95064 (1984).

58. M. J. Feigenbaum, ''The Universal Metric Properties of Nonlinear Transformations'', J. Stat. Phys. *21* (1979) 669.

59. J. P. Crutchfield, M. Nauenberg, and J. Rudnick, ''Scaling for External Noise at the Onset of Chaos'', Phys. Rev. Lett. *46* (1981) 933.

60. B. Shraiman, C. E. Wayne, and P. C. Martin, ''Scaling Theory for Noisy Period-Doubling Transitions to Chaos'', Phys. Rev. Lett. *46* (1981) 935.

61. K. Kaneko, ''Doubling of Torus'', Prog. Theor. Phys. *69* (1983) 1806.

62. K. Kaneko, ''Oscillation and Doubling of Torus'', Prog. Theor. Phys. *72* (1984) 202.

63. A. Arneodo, ''Scaling for a periodic forcing of a period-doubling system'', Phys. Rev. Lett. *53* (1984) 1240.

64. S. P. Kuznetsov and A. S. Pikovsky, ''Universality and Scaling of Period-Doubling Bifurcations in a Dissipative Distributed Medium'', Physica *19D* (1986) 384.

65. R. Kapral, ''Pattern Formation in Two-Dimensional Arrays of Coupled, Discrete-Time Oscillators'', Phys. Rev. *31A* (1985) 3868.

66. K. Kaneko, ''Frequency Locking with symmetry breaking in coupled standard map'', Prog. Theo. Phys. *69* (1983) 1477.

67. J. -M. Yuan, M. Tung, D. H. Feng, and L. M. Narducci, ''Instability and Irregular Behavior of Coupled Logistic Equations'', Phys. Rev. *28A* (1983) 1662.

68. T. Hogg and B. A. Huberman, ''Generic Behavior of Coupled Oscillators'', Phys.

Rev. *29A* (1984) 275.

69. K. Kaneko, "Phenomenology and Characterization of Spatiotemporal Chaos" in **Dynamical Systems and Singular Phenomena**, edited by G. Ikegami, World Scientific, Singapore (1987).

70. K. Kaneko, "Intermittency via Pattern Competition", in preparation .

71. R. J. Donnelly, K. Park, R. Shaw, and R.W. Walden, "Early Nonperiodic Transitions in Couette Flow", Phys. Rev. Lett. *44* (1980) 987.

72. K. Kaneko, **Collapse of Tori and Genesis of Chaos in Dissipative Systems,** World. Sci. Pub. Co., Singapore (1983).

73. Y. Aizawa, I. Nishikawa, and K. Kaneko, "Soliton Turbulence in Cellular Automata", in preparation .

74. M. Gardner, **Wheels, Life, and Other Mathematical Amusements,** Freeman, San Francisco (1983).

75. S. Wolfram, "Universality and Complexity in Cellular Automata", Physica *10D* (1984) 1.

76. T. Konishi, "Symplectic lattices", in preparation .

77. E. A. Novikov and P. W. Sewart, "Intermittency of Turbulence and the Spectrum of Fluctuations of Energy Dissipation", Isv. Akad. Nauk. USSR *Geophys. 3* (1964) 408.

78. B.B. Mandelbrot, "Intermittent Turbulence in Self-Similar Cascades: divergence of high moments and dimension of the carrier", J. Fluid. Mech. *62* (1974) 331.

79. U. Frisch, P.L. Sulem, and M. Nelkin, J. Fluid. Mech. *87* (1978) 719.

80. Y. Pomeau and P. Manneville, "Intermittent Transition to Turbulence in Dissipative Dynamical Systems", Comm. Math. Phys. *74* (1980) 189.

81. J. D. Keeler and J. D. Farmer, "Robust Space-Time Intermittency and 1/f noise", Physica *23D* (1986) 413.

82. J. P. Crutchfield, **Prediction and Stability in Classical Mechanics,** University of California, Senior Thesis, Santa Cruz (1979).

83. S. Ciliberto and J. P. Gollub, "Pattern Competition Leads to Chaos", Phys. Rev. Lett. *52* (1984) 922.

84. K. Kaneko, "Spatiotemporal Intermittency in Coupled Map Lattices", Prog. Theo. Phys. *74* (1985) 1033.

85. R. J. Deissler, "1-d Strings, Random Fluctuations, and Complex Chaotic Structures", Phys. Lett. *100A* (1984) 451.

86. R. J. Deissler and K. Kaneko, "Velocity Dependent Lyapunov Exponents as a Measure of Chaos for Open Flow Systems", Phys. Lett. A *119A* (1987) 397.

87. R. Deissler, "Spatially growing waves, intermittency, and convective chaos in a flow system", Physica D *to be published* (1987).

88. J. P. Crutchfield and O. E. Rossler, "Combinatorial Period-Doubling Instabilities and Higher Chaos", Abstract for presentation at the NATO Workshop on "Chemical Instabilities", Austin, Texas *14 March* (1983).

89. K. Kaneko, "Attractors, Basin Structures and Information Processing in Cellular Automata" in **Theory and Applications of Cellular Automata**, edited by S. Wolfram, World Scientific, Singapore (1986).

90. B. Shraiman, "Order, disorder and phase turbulence", Phys. Rev. Lett. *57* (1986) 325.

91. M. Sano, S. Sato, and Y. Sawada, private communication (1986).

92. D. Ruelle, **Thermodynamic Formalism,** Addision Wesley, Reading, MA (1978).

93. P. Alstrom and R. K. Ritala, "Mode-locking in an Infinite Set of Coupled Circle Maps", NORDITA preprint (1986).